RL-TR-97-98
Final Technical Report
June 1997

REDUCED CARRIER, HIGH DYNAMIC RANGE I/O MODULATORS

Uniphase Telecommunications Products, Inc.

Gregory J. McBrien and Glen W. Drake

APPROVED FOR PUBLIC RELEASE; DISTRIBUTION UNLIMITED.

Rome Laboratory
Air Force Materiel Command
Rome, New York

This report has been reviewed by the Rome Laboratory Public Affairs Office (PA) and is releasable to the National Technical Information Service (NTIS). At NTIS it will be releasable to the general public, including foreign nations.

RL-TR-97-98 has been reviewed and is approved for publication.

APPROVED:

NORMAN P. BERNSTEIN
Project Engineer

FOR THE COMMANDER:

DONALD W. HANSON, Director
Surveillance & Photonics Directorate

If your address has changed or if you wish to be removed from the Rome Laboratory mailing list, or if the addressee is no longer employed by your organization, please notify RL/OCPC, 25 Electronic Pky, Rome, NY 13441-4514. This will assist us in maintaining a current mailing list.

Do not return copies of this report unless contractual obligations or notices on a specific document require that it be returned.

REPORT DOCUMENTATION PAGE

Form Approved
OMB No. 0704-0188

1. AGENCY USE ONLY *(Leave blank)*	2. REPORT DATE	3. REPORT TYPE AND DATES COVERED
	June 1997	**FINAL: AUG 95 - DEC 96**

4. TITLE AND SUBTITLE
REDUCED CARRIER, HIGH DYNAMIC RANGE I/O MODULATORS

5. FUNDING NUMBERS
C - F30602-95-C-0078
PE - 63726F
PR - 2863
TA - 92
WU - 72

6. AUTHOR(S)
Gregory J. McBrien, Glen W. Drake

7. PERFORMING ORGANIZATION NAME(S) AND ADDRESS(ES)
Uniphase Telecommunications Products, Inc.
1289 Blue Hills Avenue
Bloomfield, CT 06002

8. PERFORMING ORGANIZATION REPORT NUMBER

9. SPONSORING / MONITORING AGENCY NAME(S) AND ADDRESS(ES)
Rome Laboratory/OCPC
25 Electronic Parkway
Rome, NY 13441-4515

10. SPONSORING / MONITORING AGENCY REPORT NUMBER
RL-TR-97-98

11. SUPPLEMENTARY NOTES
Rome Laboratory Project Engineer: Norman P. Bernstein, RL/OCPC, (315)330-3147

12a. DISTRIBUTION AVAILABILITY STATEMENT
Approved for public release; distribution unlimiited

12b DISTRIBUTION CODE

13. ABSTRACT *(Maximum 200 words)*

This report provides details on the fabrication and characterization of reduced carrier electrooptic modulators for potential application in high performance RF links. The report details how the optical splitting ratio was determined and the results of verification testing of reduced carrier links to prevent overload of optical detectors. The result was a slightly improved third order distortion product. This improvement could range up to 5 dB depending upon the power handling capability of the photodetector and the use and characteristics of an optical amplifier in front of the detector. The reduced optical carrier power results in an apparent increased RF modulation index (greater depth of modulation) of the optical carrier. An optical amplifier then permits higher overall optical power on the photodetector, which, in turn, improves the dynamic range of the link.

14. SUBJECT TERMS
optics, electrooptics, optical modulators, optically suppressed carrier techniques

15. NUMBER OF PAGES
60

16. PRICE CODE

17. SECURITY CLASSIFICATION OF REPORT	18. SECURITY CLASSIFICATION OF THIS PAGE	19. SECURITY CLASSIFICATION OF ABSTRACT	20. LIMITATION OF ABSTRACT
UNCLASSIFIED	**UNCLASSIFIED**	**UNCLASSIFIED**	**UNLIMITED**

TABLE OF CONTENTS

List of Figures

LIST OF ACRONYMS, TERMS AND ABBREVIATIONS

1. SFDR Spurious Free Dynamic Range - The difference in RF power, measured in $dB/Hz^{(2/3)}$, between the maximum spurious free two-tone carrier amplitude and noise floor, that can be accommodated without generating third order two-tone distortion spurs that are higher than the noise floor.
2. DOC Detector - On - Chip: The internally mounted monitor photodiode used inside the modulator package to provide measurement and feedback means for outside control and monitoring.
3. SCM Suppressed carrier modulator: A modulator topology consisting of a normal modulator bypassed by a waveguide carrying some of the incident optical power to the output where it is used to cancel some of the intensity from the inner modulator section.
4. MZ Mach-Zehnder modulator: Formed by splitting incident optical power into two waveguides, and then recombining them coherently to form an interferometric transfer function of the output intensity.
5. IP3 Intercept Point, 3rd order: This is the intercept of the fundamental, or linear response of the transfer function of the device with the line plotting the third order two tone distortion of the transfer function. This is generated by applying two RF tones to the device under test, and measuring the output amplitude of the applied tones, and the distortion spurs equally spaced on the right and left side of the two carriers. (further references in appendix A)
6. Vpi The switching voltage applied to the modulator, to advance the internal phase difference of the internal paths by 180 degrees, normally the on to off value for a Mach-Zehnder modulator.
7. E/O Electro-optic: Usually relating to a transduction of signals, applied voltage or electric field to optical intensity or phase.
8. RIN Relative intensity noise: The noise resulting from noise mechanisms of the laser source which are proportional to the laser power, that is, they scale with the laser power, usually measured in a 1 Hz bandwidth. Typical values for analog links are from -165 to -175 dBc/Hz, measured with respect to the detected DC power.
9. "F" parameter: The front-end tap ratio, of the split off power diverted from the inner Mach-Zehnder, which establishes the portion of optic intensity to be used for cancellation at the output.
10. ILS Integrated Logistics Support: Methodology to support the deployment, maintenance, repair, and general field use of the device.
11. SOW Statement of Work: The defined tasks for the contract
12. IOC Integrated Optic Circuit: The optical device, typically Lithium Niobate, upon which optical circuits are laid out to perform a modulation or other function.
13. SM Single-Mode: Waveguide, typically fiber, supporting only one propogation mode, in the case of fiber, because of its small core diameter.
14. RF Radio Frequency: High frequency electromagnetic signals, usually greater than 10 MHz.

15. DC Direct Current: Current or voltage which is non-zero, and not time-varying.
16. AC Alternating Current: Current or voltage which is non-zero, and is time-varying, usually sinusoidal with time.
17. S/N Serial number
18. YBBM Y bridge balanced modulator: A modulator with an input Y branch, and downstream combining junction of the waveguides to provide two complementary outputs.
19. CATV Community Access Television: Broadband video broadcast services, carried by either electrical cable or fiber optic cable.
20. OMI Optical modulation index: The ratio of the zero to peak Ac waveform to the average DC level of the waveform.
21. YAG Yittrium-Aluminum-Garnet: A laser, typically pumped by another semiconductor laser, having light emission at either 1319, or 1338 nm wavelength.
22. Pout Pout: Power, typically RF or optic, out of a signal node
23. Pin Pin: Power input, typically into an RF or optic signal node
24. Idc DC electrical current, usually measured in milliamps, or amperes.

REDUCED CARRIER/HIGH DYNAMIC RANGE I/O MODULATORS

EXECUTIVE SUMMARY

The use of external modulators having sinusoidal transfer functions based on simple two-arm Mach-Zenhder modulators has become commonplace for military and commercial applications. These products are mature, and well understood. Development activities at a variety of commercial and government sites presently focus on newer, more complex external modulator topologies, such as cascaded, paralleled, and "nested" configurations. The more complex modulator topologies explored here focused on carrier suppression, which is implemented by adding an end-around path around a Mach-Zenhder modulator, recombined at the output to modify the device transfer function into a non-sinusoidal output.

This program investigated the issues of characterizing and fabricating these more complex modulators for analog applications. 5 devices were built, packaged, and tested at 1310 nm and 1550 nm. Breadboard electronics were used to control the device operating point, by using internal photodiode monitoring that was built into the package.

For multi-octave applications where second and third order distortions are important, the configurations yielded comparable SFDR test data to theoretical SFDR of a simple modulator, when the photodetector current was normalized. A possible advantage was seen in the slightly lower third order derivative in the transfer function at the second derivative null point, when the linear slope was normalized to a comparable Mach-Zenhder. This lower third order derivative may imply lower third order distortions which might imply lower third order two-tone distortion.

PROGRAM SUMMARY

Motivation

Increased dynamic range for analog microwave systems is required in order to detect very weak signals in the presence of very strong ones. Optic links for microwave systems have demonstrated high dynamic ranges but even more dynamic range is needed for some important applications.

In order to increase the dynamic range of externally modulated wide band microwave optic links one of the issues that must be addressed is the limit on how much optical power the photodetector can absorb before it becomes non-linear or physically damaged. Since the dynamic range of an externally modulated optic link is strongly related to the amount of optical power used optic link designers are often in search of photodetectors that can perform well at higher optical power levels. At the present time detectors that work at frequencies of 20 GHz, for example, will become nonlinear at a level of only a few milliwatts of incident optical power. This limits the possible spurious free dynamic range of the link to around 110 $(dB/Hz)^{2/3}$.

Recent studies have indicated that dynamic range enhancement can be achieved by reducing the level of DC optical carrier while leaving the information sidebands intact. Then, for the same total power on the detector more of the energy is in the sidebands and less in the optical carrier. This leads to increased dynamic range for the system.

Experiments to demonstrate this have been performed using very narrow optical filters.[1] Although increased dynamic range has been shown the optical filters are very difficult to fabricate and are very unstable with temperature.

External modulators can be designed to reduce the optical carrier of the output by using a branch structure to split off some of the input optical carrier, and coherently reduce the optical carrier at the output. A number of design issues relating to modulator fabrication and bias point control result from these approaches.

Program scope

This program consisted of the design, fabrication and testing of integrated optic modulators that consisted of a Mach-Zehnder modulator and a phase modulator in parallel on a single lithium niobate substrate. Some of the input optical carrier was sent through the phase modulator and recombined with the signal at the output of the M/Z modulator to cancel some of the optical carrier. It was necessary to leave some optical carrier for signal recovery at the detector. Determining the optimum operating conditions for the arrangement was the subject of the experiments. The scope of this work included fabrication of devices at 1.3 and 1.5 um operating wavelength, at frequencies out to 18 GHz. Bias control electronics were designed using photodetectors mounted internally inside the modulator package. Test and analysis included evaluation of the resulting link Spurious Free Dynamic Range, (SFDR) for normal modulators and carrier reduced modulators. Bias point, loss, and RF response characteristics were also measured.

Deliverables (SOW line items:)

The following items are derived from line items in the statement of work. The line item numbers have been repeated as they appear in the SOW. (Some intermediate step items are not stated for brevity. The intermediate steps' completion is implied by the completion of the stated tasks)

4.1.1 Modeling: Develop a mathematical model to determine the optimal amount of dynamic range possible for a variety of laser power levels and detector power handling capabilities.

4.1.2 Testing: Test bias control, carrier suppression circuitry, and the prototype modulators

4.1.3 Control Circuit Design: Design a bias control circuit using photodiodes mounted integrally to the modulator, as well as carrier suppression point control circuit.

4.1.4 Advanced Suppressed Carrier Modulator Fabrication:

4.1.4.2 Fabricate and test two sets of advanced technology modulators.

4.1.4.3 Fabricate, and test ,after iteration, two modulators for operation at a wavelength of 1300 nanometers, and two reduced carrier modulators at 1550 nanometers.

4.1.5 Package Design: Design the packages for the modulators using custom packages modified for the additional DOC's, connectors, and additional length of the device.

4.1.6 Fabrication and Assembly. Integrate the packaged carrier modulators into systems for testing including breadboards of the bias and carrier suppression control, and including lasers, fibers, and detectors to construct a test bed system.

4.1.7 Integrated Logistic Support (ILS). Address reliability, Maintainability, Supportability, Operating requirements, and Environmental requirements.

BACKGROUND

The demands of high performance microwave electronic and fiber optic links require higher dynamic range to allow the detection of weak signals in the presence of interference. In fiber optic systems one of the most notable limitations for high dynamic range in broad band or high frequency systems is the fact that high frequency photodetectors have a small active area to keep capacitance low and thus cannot handle high optical power levels.

Fiber optic links that use external modulation exhibit a dynamic range characteristic that increases with optical power level. Higher dynamic ranges are possible if the detectors could handle more optical power. However, the signal that comes out of the external modulator is largely unmodulated optical carrier with fairly small information sidebands. The small signals are required because the external modulator is linear over only a small portion of its transfer function.

Preliminary analysis indicates that feeding some unmodulated optical carrier forward will allow cancellation of some of the optical carrier while leaving the information sidebands intact. This would allow higher information power levels at the detector and higher dynamic range for the system.

A similar technique has been tried by others[1] using very narrow optical filters to suppress the optical carrier while leaving the sidebands intact. Test data from these experiments have shown increased dynamic range. However, the optical filters used were very unstable over temperature.[1] One advantage of feeding forward a cancellation intensity in an additional path of an external modulator is that the reduction in amplitude of the optical carrier is performed by a means that is potentially stable. It is the goal of the IOC designer to choose topologies and operating points that provide the desired performance increase with the widest parameter tolerances possible. Biasing of simple Mach-Zehnder interferometers at their operating point has received much attention in the development of external modulators. Here, controlling the bias point of the carrier-reduced modulator warrants some investigation.

Increasing the laser optical power output while reducing the optical carrier level at the receiver should yield an SFDR increase of about 5dB for a link with a preamplifier.

Since there will be 3 dB more optical loss through the Mach-Zehnder modulator than through the phase modulator leg the optical splitting ratio at the input should not be a 50/50% split. More light should be allowed to travel through the Mach-Zehnder part of the device.

This technique could also be used to reduce stimulated Brillouin scattering in long lengths of SM fiber by reducing the total optical power in the fiber while keeping the modulated optical power at the same level.

The inner Mach-Zehnder is unchanged from a standard device with bias and signal electrodes appropriate for the required bandwidth. The optical carrier phase shift electrode is identical to the bias electrode and will serve a similar function.

Bias Control

The bias control for the inner M-Z modulator is done in the standard manner, minimizing the second harmonic, using the detector on chip at the end of the M-Z for the bias point feedback. Alternatively, if the Y-fed balanced bridge modulator is used a dual detector on chip scheme could be used.

For the optical carrier suppression there is also a DOC for feedback. In this case, however, the feedback is used for AGC type operation where the optical carrier bias is adjusted to obtain the desired output signal level.

ANALYSIS / MODELING

Detection issues

The detector is a square law device that mixes the optical carrier with the sidebands to recreate the input signal frequency. If we represent the optical carrier signal as $V_o(t) = A\sin(\omega_1 t)$ and the information sideband signal as $V_s(t) = B\sin(\omega_2 t)$ then the signal at the detector becomes:

Eqn. 1. $$V(t) = \left(A\sin(\omega_1 t) + B\sin(\omega_2 t)\right)^2$$

This expands to

Eqn. 2. $$V(t) = A^2\sin^2(\omega_1 t) + AB\sin(\omega_1 t)\sin(\omega_2 t) + B^2\sin^2(\omega_2 t)$$

The middle term yields in part the term

Eqn. 3. $$\frac{AB}{2}\cos\left((\omega_1 - \omega_2)t\right)$$

This is the desired baseband frequency term and we can see that its amplitude is proportional to the product of the amplitudes of the carrier and sideband signals. For a 3% modulation depth, B = 0.03 x A. For a fifty percent modulation depth, B = 0.5 x A. If the total power incident on the photodetector is held constant the AB product for the 50% modulation case is about 9 times greater than the 3% modulation case which means the RF signal voltage across the detector load has been increased by a factor of nine.

Source Factors

Since the input optical carrier signal is split, very high power optical sources (in the range of 500 milliwatt) are required to achieve significant SFDR improvements. Also, although the SFDR of the optic link increases there is still a significant noise figure. The use of a preamplifier in front of the link to reduce the noise figure reduced some of the SFDR improvement.

Reduced Carrier Modulator Concept

The topology for a suppressed carrier modulator can be constructed from Figure 1, analysis by Bridges [2], and others [3]. the coupler structures and electrodes are shown symbolically for simplicity.

Optical carrier reduction at the output of an integrated optic device can be achieved by feeding forward some of the unmodulated input optical carrier and recombining it at the output of the device. It should be possible to split the incoming optical signal and re-combine it at the output nearly 180 degrees out of phase such that the optical carrier is reduced at the output of the modulator. The figure shows a Mach-Zehnder modulator being used to modulate the signal but a Y-fed balanced bridge modulator could also be used. The unmodulated optical carrier, Ein, is fed into the modulator structure at the left. The upper path is sent to an RF-modulated Mach Zehnder interferometer, where small signal modulation is typically fed into the signal electrode. At this point, the output contains optical carrier, with information carrying sidebands fo + fs, and fo - fs. The output is then routed to a combining node of an outer MZ, where a portion of the original optical carrier is interfered to reduce the optical carrier.

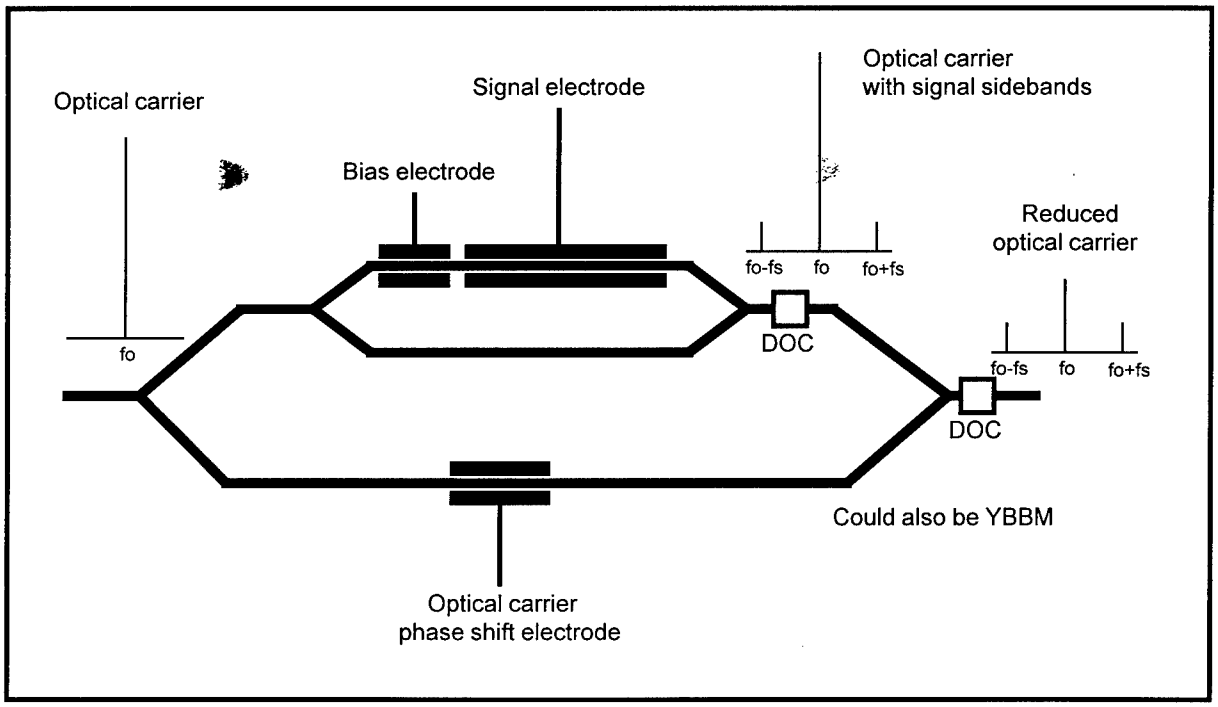

Figure 1. Conceptual drawing of reduced carrier I/O modulator.

The approach taken was to first create predictive models of the performance of the reduced carrier modulators, then design and fabricate modulators based on the indications of the predictive model of what the optimal physical dimensions and characteristics of the device should be, then to test and compare the actual performance of the reduced carrier modulators to the predicted performance values especially with regard to dynamic range characteristics.

Two iterations of the design and fabrication process were performed to facilitate an optimization of the device parameters. Table 1 shows an outline of the proposed approach.

Transfer function

The transfer function of the carrier suppression results from the summation of the electric fields from the modulated MZ, and the "power bypass" leg, or DC cancellation leg. A mathematical model was constructed and modeled on Mathcad to show the transfer functions. Families of curves exist, because the front-end tap ratio, used here as "F", can be varied, shifting the portion of power between the modulated path and bypass path. Additionally, the bypass path can have its phase varied with respect to the modulated path. The characteristic equation is derived by solving for the respective leg intensities, I1, I2, and Io:

$$I1 := Ein^2 \cdot F + Ein^2 \cdot F \cdot \cos(2 \cdot \phi)$$

$$I2 := Ein^2 \cdot (1 - F)$$

Combining I1 and I2:

$$Io := Ein^2 \cdot F \cdot (1 + \cos(2 \cdot \phi)) + Ein^2 \cdot (1 - F) + 2 \cdot Ein^2 \cdot \sqrt{1 - F} \cdot \sqrt{F} \cdot \sqrt{1 + \cos(2 \cdot \phi) \cdot \cos(\Phi)}$$

Collecting terms and simplifying yields:

$$Io := \left[2 \cdot F \cdot \cos(\phi)^2 + 2 \cdot \sqrt{F \cdot (1 - F)} \cdot \sqrt{2} \cdot \cos(\phi) \cdot \cos(\Phi) + 1 - F \right] \cdot Ein^2$$

For a normal Mach-Zehnder, the zero order, fundamental, second, and third order response can be compared. This is shown here;

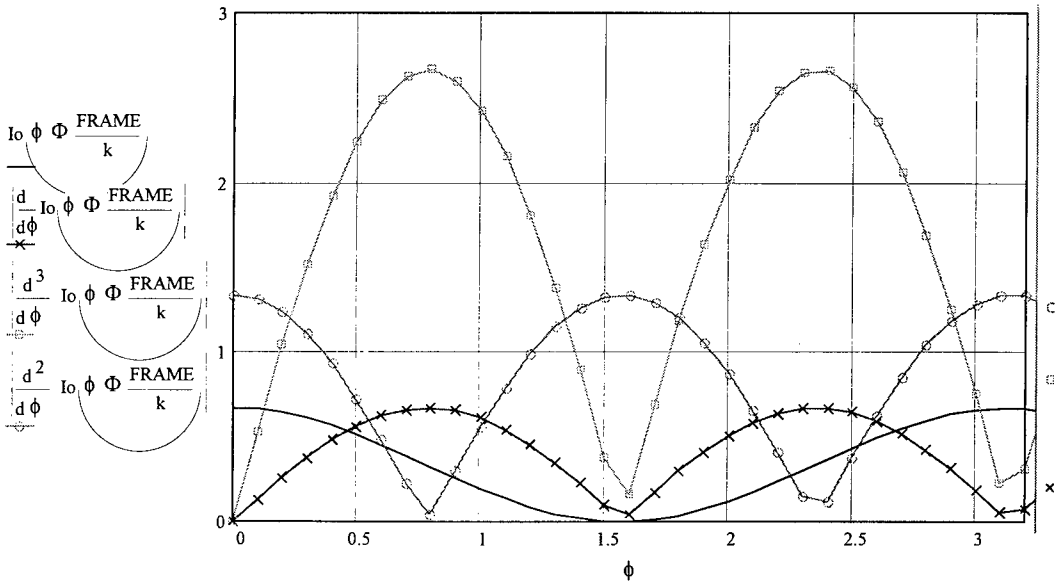

Figure 2: Mach-Zehnder Transfer Function, and Derivatives

This shows the "classic" relationship of Mach-Zehnders, the normal operating point is where the fundamental is maximized , (at the half power point). The third order, and all odd order

derivatives are maximized at the same point where the second order derivative is nulled. This of course is the reason, CATV, broadband antenna remoting, and other applications always use the modulator at the half power point.

The transfer function was evaluated for the carrier suppressed modulator with an "F" value of .6667, at a phase angle of 0 degrees, and derivatives plotted for the transfer function. The first, second, and third derivatives imply the magnitude of the RF fundamental, second harmonic distortion, and third harmonic distortion. The transfer function was also evaluated for different phase angles to investigate the shapes for possible implementation. One difference in the carrier suppressed modulator was that at the second order derivative null, the ratio of third harmonic to first harmonic was somewhat different, which should imply different IP3, and SFDR characteristics. This was evaluated in the testing.

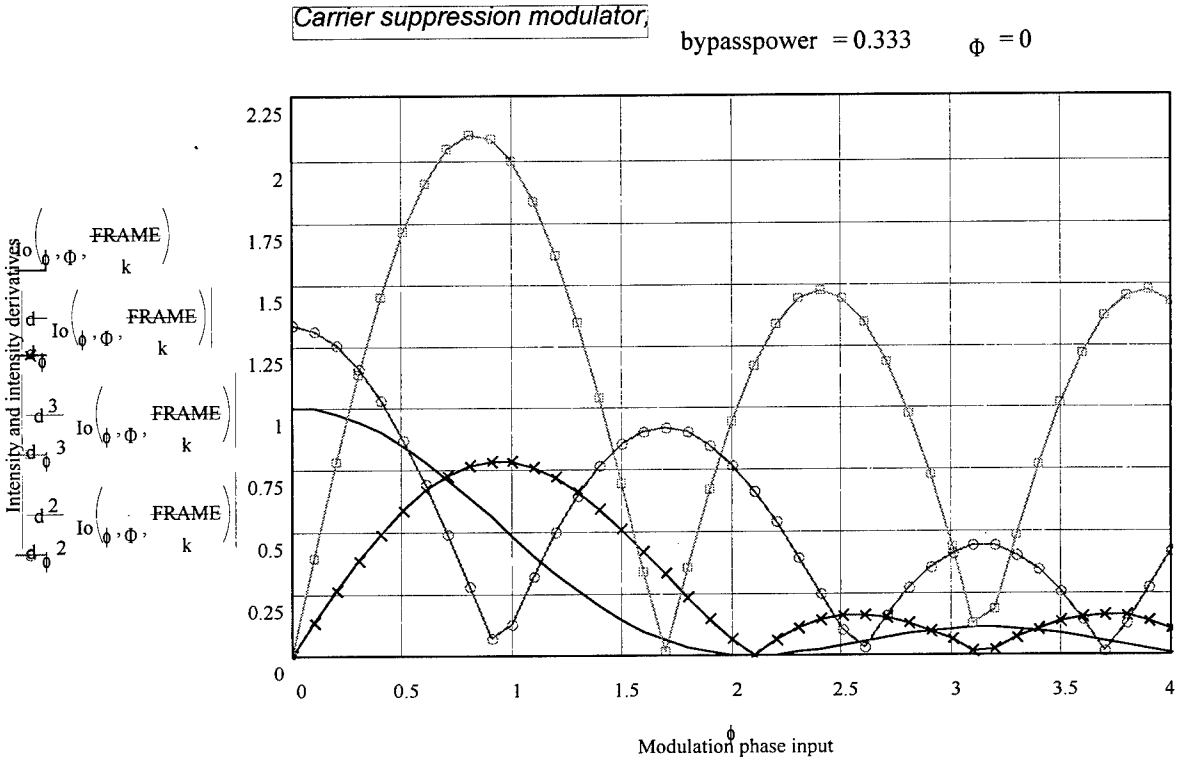

Figure 3: Carrier Suppression Transfer Function, and Derivatives

For carrier suppression bypass power fixed, varying carrier suppression "DC" phase yields a family of transfer functions: These curves are shown with the input power split of .667 to the Mach-Zehnder modulator, and .333 to the bypass leg. The zero degree phasing preserves the best extinction ratio.

bypasspower = 0.333

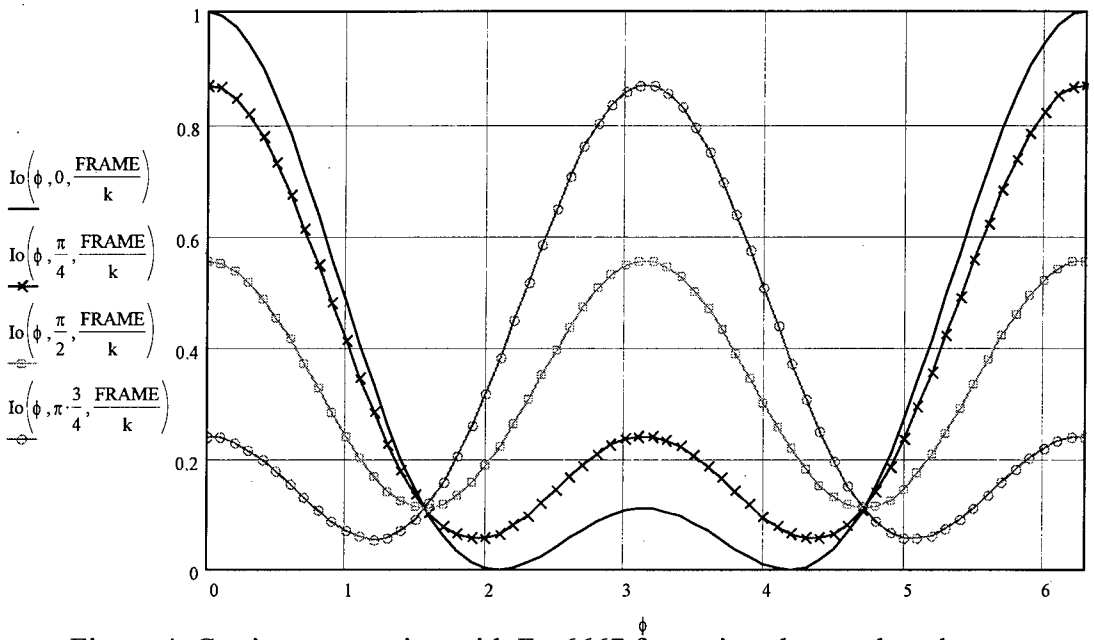

Figure 4: Carrier suppression with F=.6667 for various bypass leg phases

DESIGN

In the first phase, two different wavelengths and two different topologies were investigated. Design wavelengths were at 1320 nm, and 1550 nm. A diagram of the devices is shown in figure 2. 67% and 33% intensity splits were used to allow up to full carrier cancellation at 180 degrees of phase.

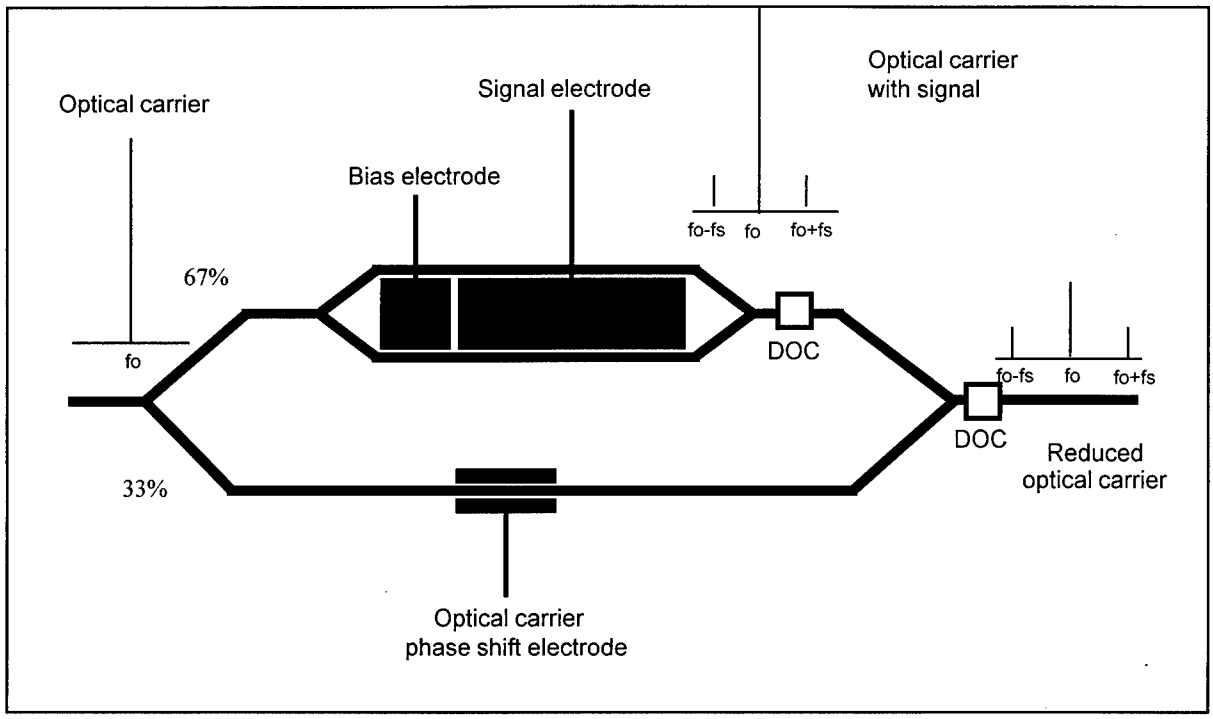

Figure 5, 1st iteration device

This device used standard 6 GHz electrode structures similar to ones used in other UTP products. Photodetector-On-Chips, "DOC's" as they are known by, from a proprietary UTP process were integrated into the first Y branch of the "inner" MZ, and one placed on the carrier reduced output leg. These photodiode monitoring elements provided flexibility in the biasing method. The "DOC" currents could also be scaled and differenced to control the amount of carrier reduction. A suitable control was designed with the following topology, using nulling circuits to balance the DOC output currents, shown here in figure 6:

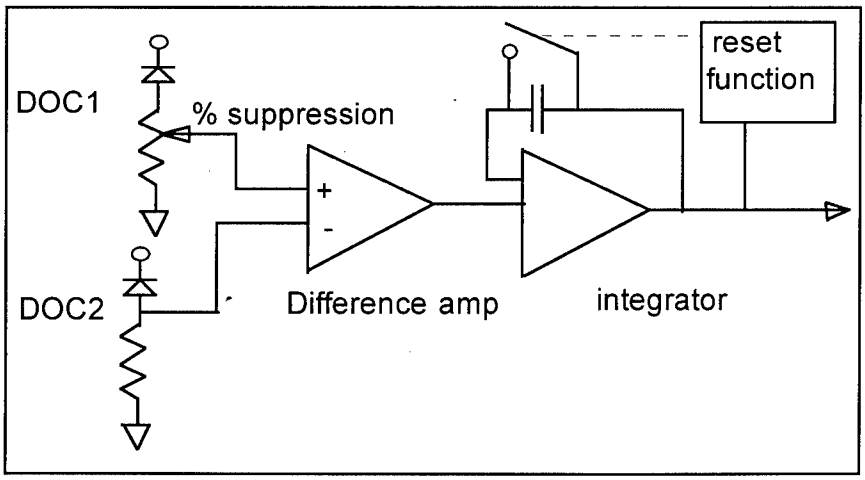

Figure 6, Carrier suppression control circuit with on-chip-photodetectors

A second device was designed. Additional features were included. The electrode structure was changed to an 18 GHz modulator electrode structure. The "inner" modulator was changed to a Y bridge balanced modulator, with dual output. This was done for two reasons: By adding an additional photodetector, bias control of the "inner" modulator was easily controlled. Second, the extra leg of the inner modulator was useful for testing to compare and monitor the behavior of the inner section while operating the composite structure. Finally, a traveling wave phase modulator was added to provide flexibility in applications requiring spectral broadening. The DC electrode was eliminated by using a bias "tee" on the RF electrode. Figure 7 shows this structure:

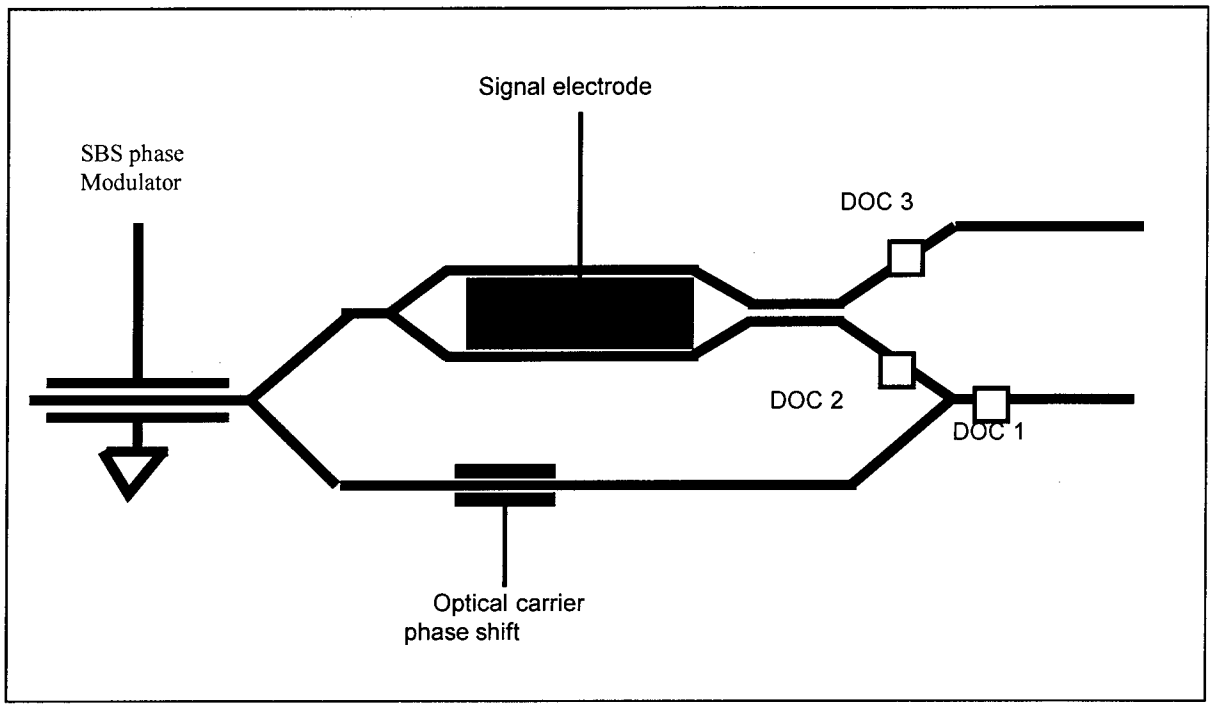

Figure 7, Second iteration modulator with 3 DOC's

FABRICATION

Two sets of devices were fabricated. They were built and packaged using standard UTP design rules and packages. Both iteration devices used similar packaging, so externally, they look the same. The packages resembled the standard 18 GHz modulators that UTP produces, with the exception of added connectors, and dimensions changed internally to accommodate the carrier suppression topology. Microstrip ceramic substrates were designed and laid out internally to interconnect the RF and DC electrodes. A picture of the device is shown here in Figure 8:

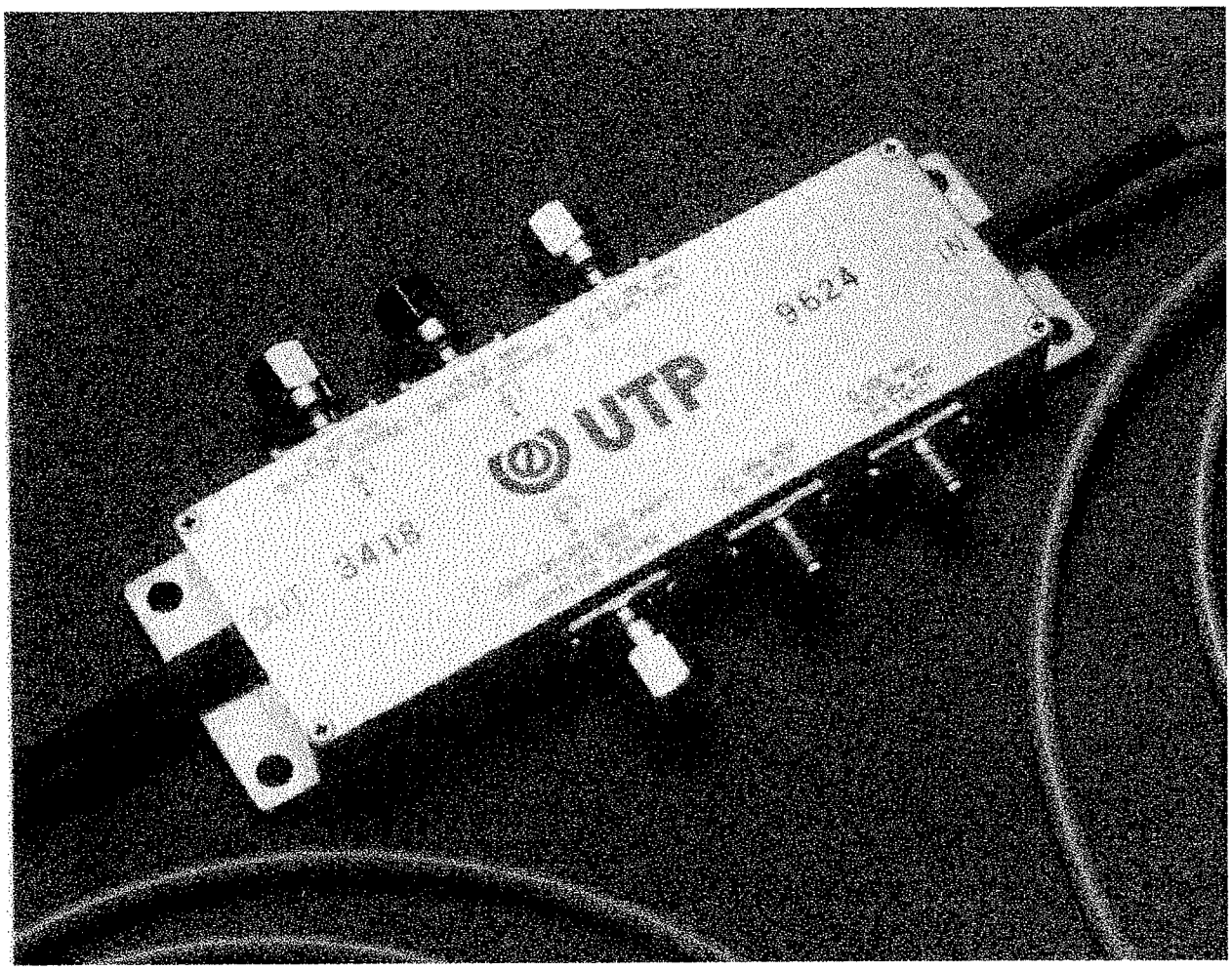

Figure 8: Carrier Suppressed Modulator, in package

TEST RESULTS

First Iteration Devices

The first iteration devices were tested using a 1310 nm YAG laser and HP photodetector using both breadboarded bias control electronics and manual bias settings. The photodiode outputs were monitored as the carrier reduction point was set at various levels by way of the phase adjustment between the modulation leg and the "bypass" leg. The second order distortions from the modulator were kept at a null. The two plots, figures 9 and 10 show the actual and analytical data from the evaluations of the device, respectively.

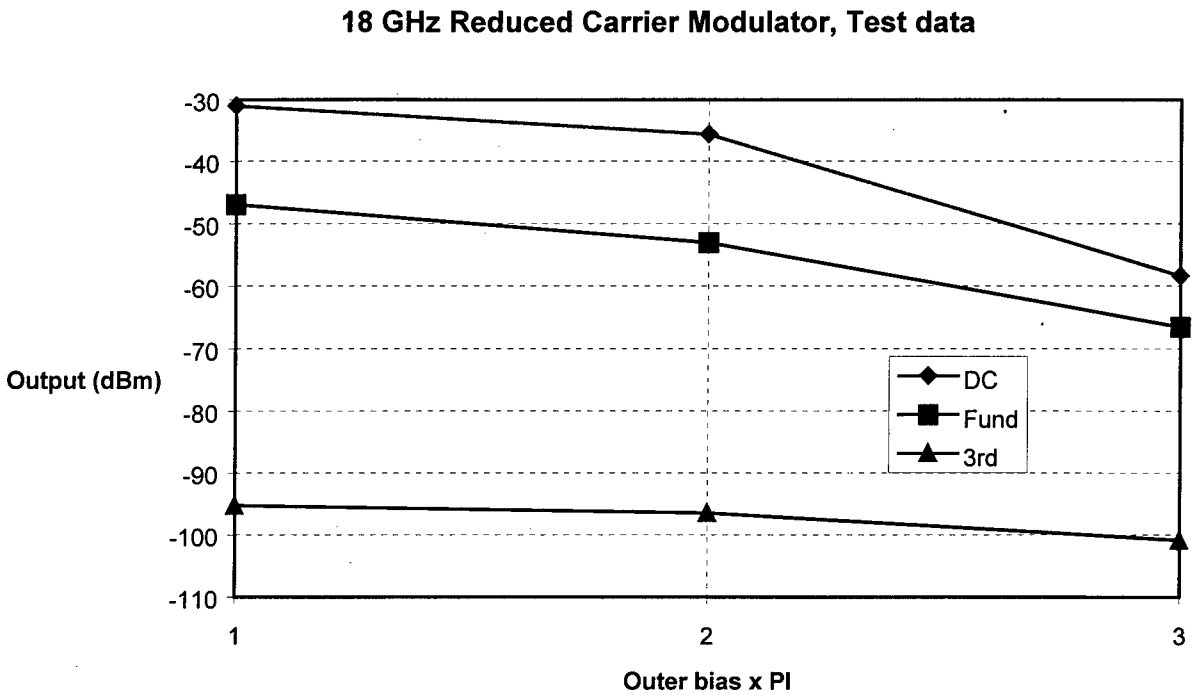

Figure 9, Reduced Carrier Modulator data

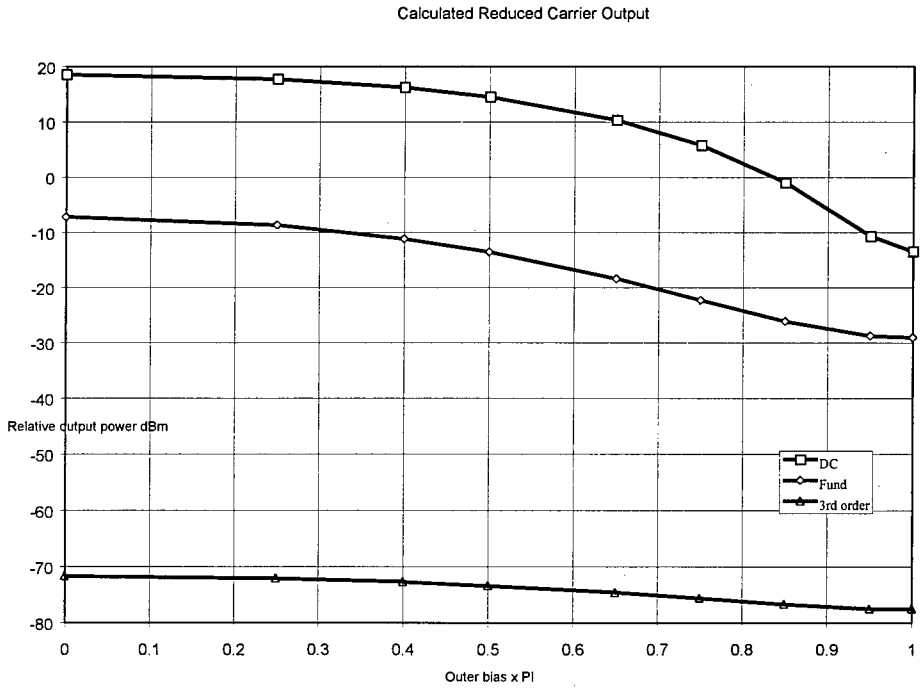

Figure 10, Reduced Carrier Calculated Behavior

Under these conditions, the reduction of the optical carrier was accompanied by less of a reduction in the fundamental output term, which was good. However, even less of a reduction of the third order two-tone spur occurred. This opposed the gains seen by reducing the optical carrier. In one case the optical power dropped 32 dB, the RF fundamental tone dropped 22 dB, and the third order two tone dropped 6 dB.

The SFDR calculations for a "simple" Mach Zehnder modulator compared with the carrier suppressed modulator were as follows: With .17 milliwatts on the link photodetector, 50 ohm detector impedance, and 25 ohm modulator impedance, and Vpi of 3.1 volts, the calculated SFDR of the simple MZ was:

Link Gain = -45.6 dB (no preamp)

Noise Figure = 47.6 dB

IP3 output = -23.7 dBm

SFDR = 98.8 (dB/Hz)^2/3

For the carrier suppressed modulator, the data was as follows:

Link Gain = -55.4 dB

Noise Figure = 57.4 dB

IP3 output = -24.8 dBm

SFDR = 98.1 (dB/Hz)^2/3

Second Iteration Devices (testing)

The second iteration devices, consisting of two devices at 1.3 um, and two at 1.5 um, were tested. The focus of the second iteration device evaluation was to investigate some other potentially relevant areas, such as ability to bias control a "composite" modulator structure, and also investigating the general transfer function, as well as SFDR measurements. Additionally, these tests were repeated on the first iteration devices as a comparison.

The following table, Figure 11, summarizes device characteristics for both the first and second iteration devices:

Serial#	Loss, chip	Loss, pigtailed	On/Off	Vpi (RF)	Vpi (Bias)	Test Wave	Job#	Sliver ID
First iteration								
SC001	2.85 dB	<6dB	17.88	12.91	4.56	1319 nm	1003B	2225-2-D
Second iteration								
SN3418	3.12 dB	4.66 dB	22.00	13.00	5.00	1319 nm	1124A	2476-1-C
SN3421	3.30 dB	4.86 dB	22.40	13.21	4.90	1319 nm	1124A	2476-1-D
SN3423	3.10 dB	4.41 dB	15.60	15.00	5.50	1548 nm	1124B	2527-1-E
SN3419	3.10 dB	4.47 dB	15.10	15.50	5.40	1548 nm	1124B	2527-1-F

Figure 11: Table of Individual modulator characteristics

The devices were characterized for large signal operation. This included sweeping out the RF electrode response with a low frequency triangle wave, and measuring third order two tone spurs at a given OMI (optical modulation index). The devices did have the characteristic transfer function plotted analytically in the preceding sections. For device S/N SC001, the a plot of the transfer function is shown here:

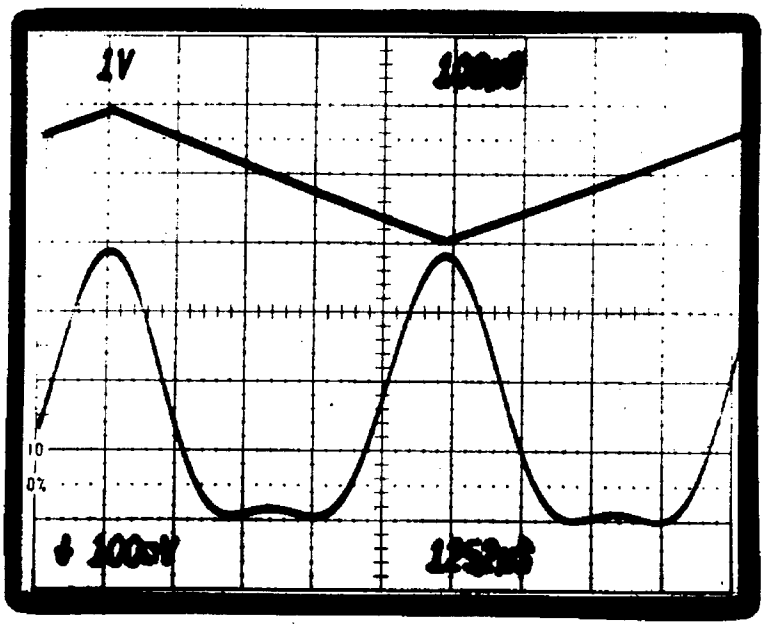

Figure 12: Carrier suppressed modulator transfer function data

The device exhibited a very different characteristic than a "normal" Mach-Zehnder modulator. It did show the repeated minor local maxima peak predicted by the analysis. This plot was generated with the suppression leg phase set to 0 degrees. This was attained experimentally by varying the voltage on the phase electrode and finding the maximum on/off extinction. It is also anticipated that since the "zeroith" order transfer function shape follows the analysis, then the first, second, and third order derivatives will follow as well, yielding the small signal gain, second order distortion, and third order distortion characteristics of the structure.

The voltage was then varied to approximately 180 degrees offset, and another characteristic resulted; the shape was the same, with the peaks reversed with respect to the input triangle wave, this is shown in figure 13:

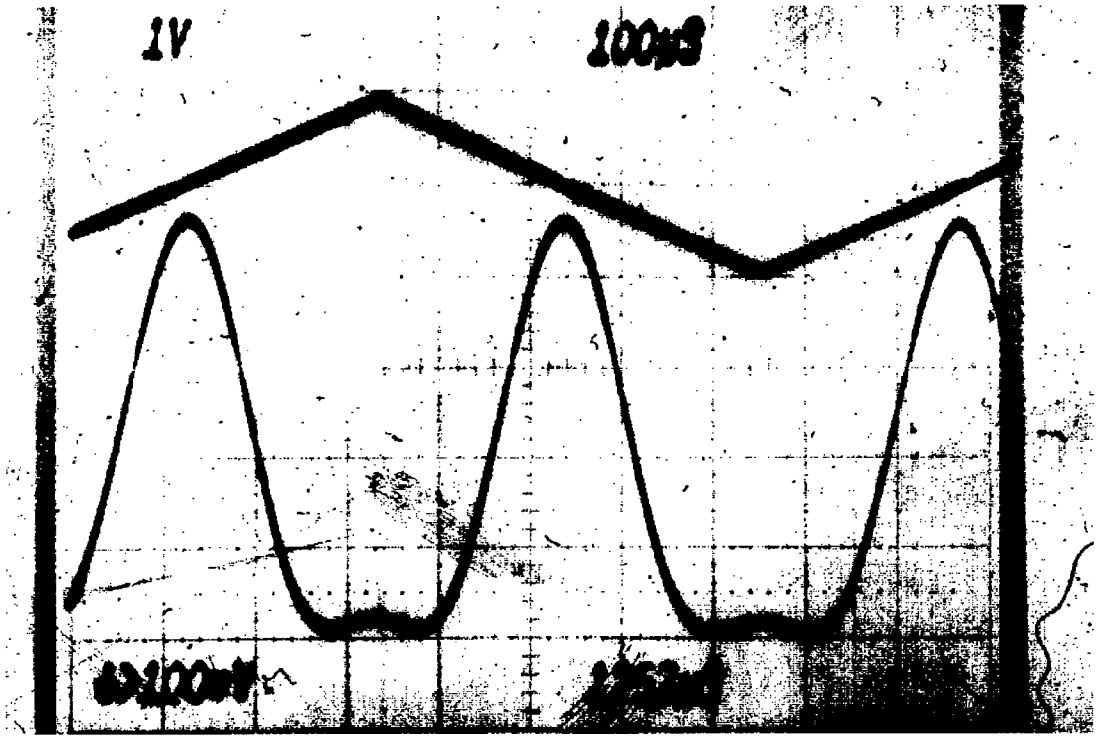

Figure 13. 180 degree offset transfer function

The same transfer function resulted, with the local maxima occurring at the triangle input peak positive voltage. This resulting shape of the transfer function reveals the difference between what one would envision as a carrier suppressed modulator, that is a sinusoidal modulation transfer function with the "DC" suppressed, and the actual result of feeding forward some of the unmodulated carrier. A better description of this topology would be one of a "nested" modulator, where the modulated power from a MZ structure is re-interfered with another intensity branch. This re-interference explains the apparent fourth-order behavior with the second local maxima. The transfer function has similarity to other cascaded modulator structures reported by Betts [4], and others.

Testing was performed on the first iteration device to evaluate the two-tone distortion characteristics. This data was taken with intentionally large side spurs, on the order of 60 dB with respect to the RF carrier. Data was taken with the carrier suppression leg set at 0 degrees of phase, and 180 degrees of phase. The bias point of the internal "MZ" was set to maintain the second order distortion null of the composite structure. The distortion characteristics at a given modulation index were compared to that of a normal MZ. Of course, to perform a meaningful measurement, accurate knowledge of the modulation index must exist. A normal MZ has predictable third order distortion behavior, since the third order distortions result from the series expansion of the sinewave characteristic. The following equation was used to calculate expected distortions for a given OMI:

$$\Delta_{avg} = 20 \log\left(\frac{OMI^2}{8 - 3OMI^2}\right) \text{ dBc}$$

This equation relates the amplitude of the third order two-tone side-spurs, to the modulation index of each of the two RF tones applied to the input port of the modulator. Refer to the appendix for the derivation of this equation.

Figure 14 shows the output from the modulator after detection by a broadband HP photodiode. The two tones were applied near 2 GHz, and the adjacent side-spur plotted. This was taken with the phase of the suppression leg at zero, with full suppression. The DC value on the detector was .212 ma.

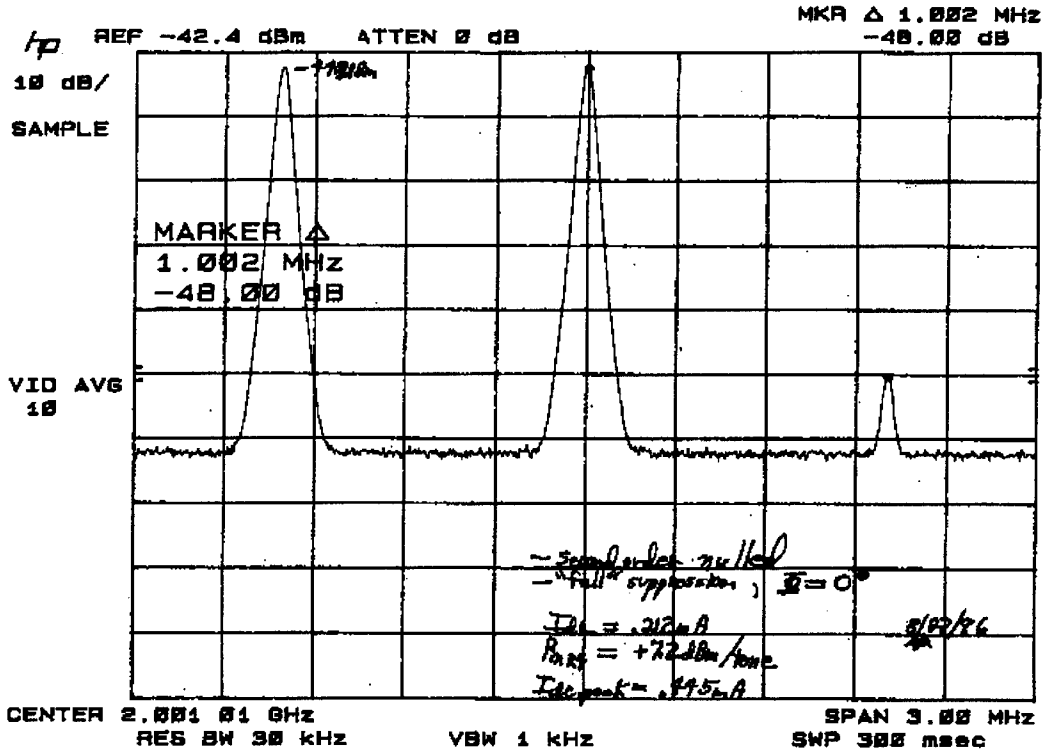

Figure 14, Two-tone intermod test with "full" suppression

From the plot, the output carriers were at -44.3 dBm, with the sidespur 48 dBc. The input RF power was 7.2 dBm per carrier. Vpi and OMI can be calculated from this. Using the OMI equation in the previous section, the OMI was calculated to be 17.78%. If we use the DC photocurrent and output carrier level to calculate the OMI from the AC/DC ratio, then the result would be: Iac/Idc. The AC carrier is the -44.3 dBm value, and the DC part is the photodetector .212 ma. This ratio, with some conversion of the AC RF power to peak AC photocurrent, is 18.25%. This is slightly better than a simple MZ, but also within measurement accuracy. As will be reported in the following sections, RF loss from the photodetector required some calibration, since attenuation of the RF carrier output compared to the non-lossy DC transmission affects the AC/DC ratio method of OMI measurement. (see appendix).

Vpi for this modulator was calculated, knowing the RF carrier input level, (+7.2 dBm), and the OMI, 17.78%. This measurement yielded a value of 12.8 volts, in reasonable agreement with the device data measured at chip fabrication.

The two-tone test was then repeated for a carrier suppression phase of 180 degrees. This is shown in figure 15:

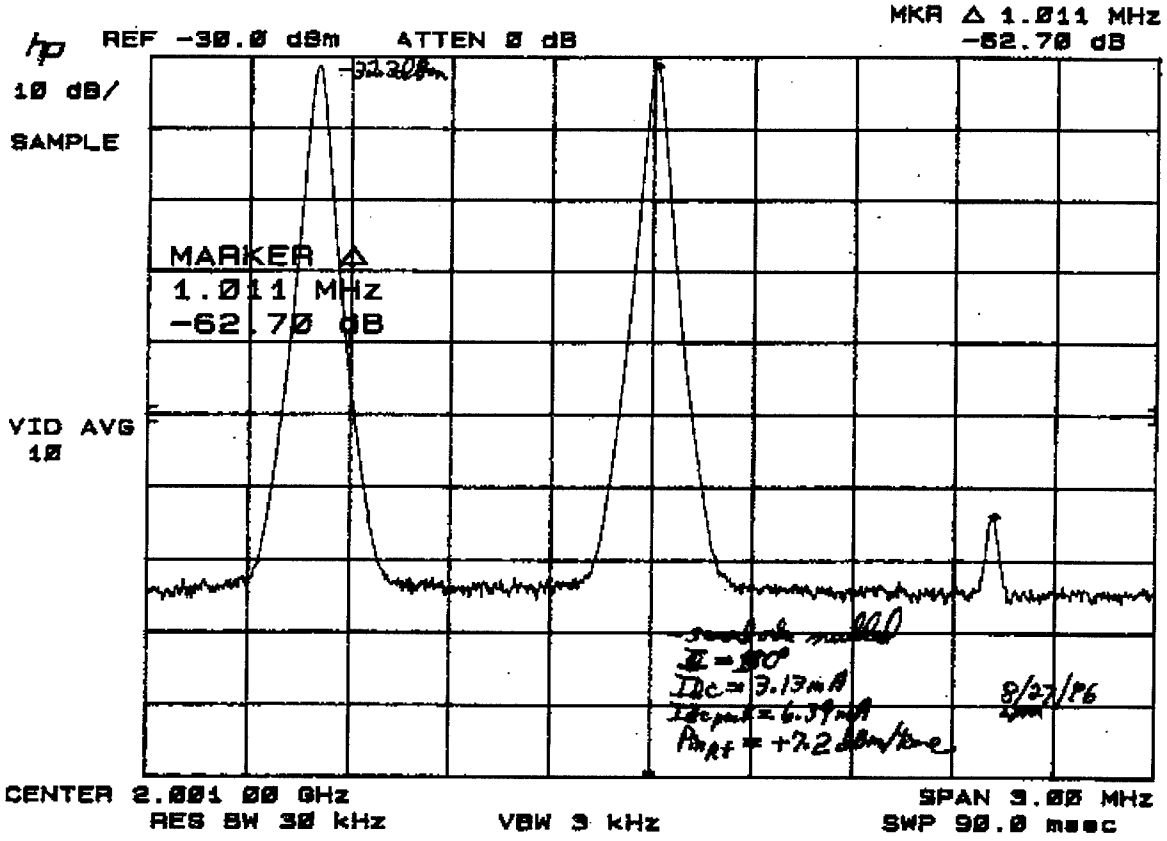

Figure 15, Two tone test with carrier suppressed phase of 180 degrees.

The second order distortion was nulled, and DC photocurrent, RF fundamental, and side tone delta measured. It was interesting to see that this provided a new set of data with the same second order null. The carrier measured was -32.3 dBm, DC photocurrent of 3.13 ma, and a distortion side tone of -62.7 dBc. This yields a simple MZ ,two-tone spur calculated OMI of 7.63%. Using the AC/DC ratio method, (valid for any transfer function), a value of 4.91% is calculated. This result is much different than that of the previous plot. For these settings a comparable spur level equates to a 3.8 dB worse OMI than a simple MZ.

Since the modulator topology has different bias points for harmonic nulls, as reported by Bridges[1] , and others, a test was performed to verify the third order null existence. This is shown in figure 16 , before and after movement of the bias point to null the two-tone distortion. One case shows the spur levels with the second order nulled, the second plot shows the two-tone distortion nulled with non-zero second order distortion. Of interest is that the RF carrier is depressed approximately 9.4 dB. The bias point was varied on both sides of the null to verify that the distortion product passed through a distortion null.

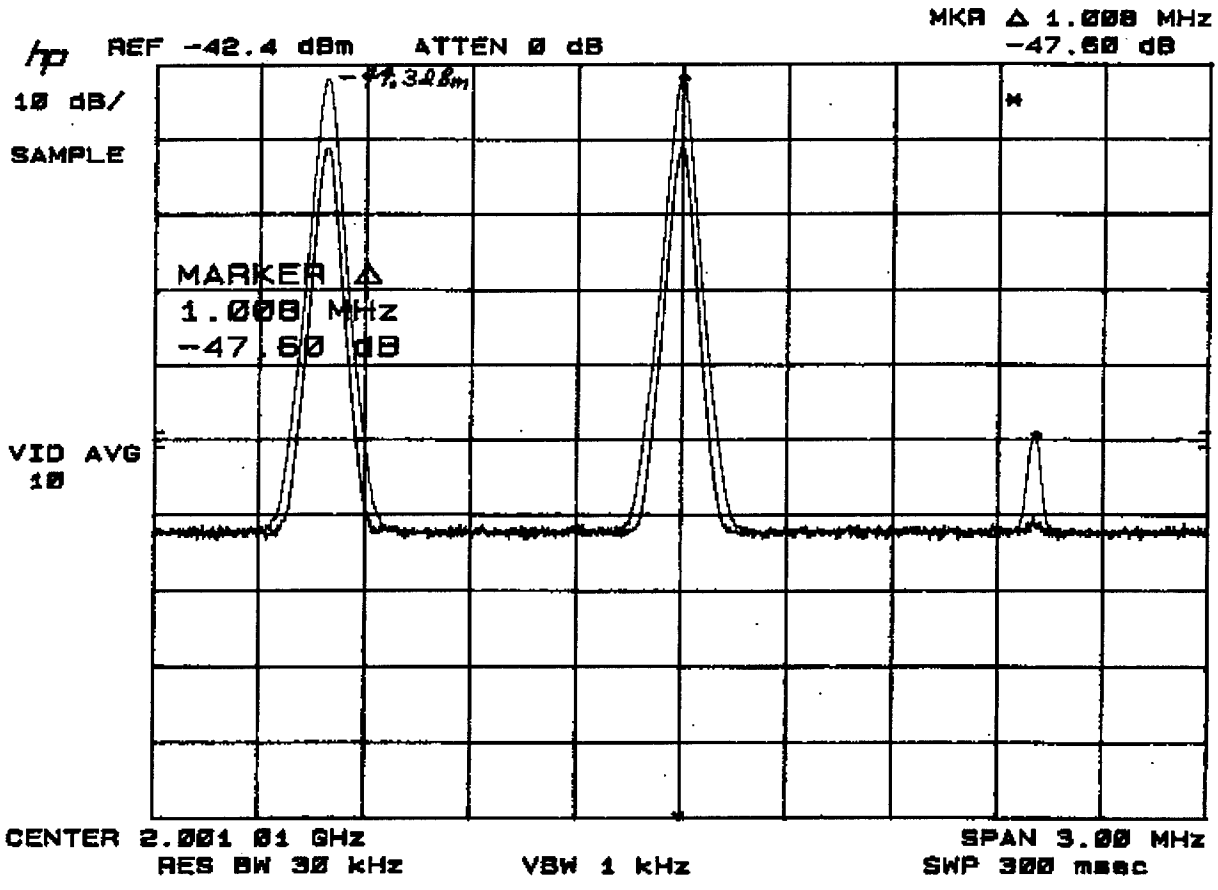

Figure 16 Existence of the third order two tone null

The same series of measurements were carried out on SN3418, of the second iteration devices. This modulator offered several advantages. The modulator had a "normal" MZ output, so a comparison was made with the carrier suppressed output. The modulator had internal photodetector-on-chip mounted, which was used to run the internal bias control. The modulator also had lower loss than the previous iteration. The transfer function was mapped for the normal MZ, in the following plot, figure 17. The transfer function was, as expected, a simple sinusoid:

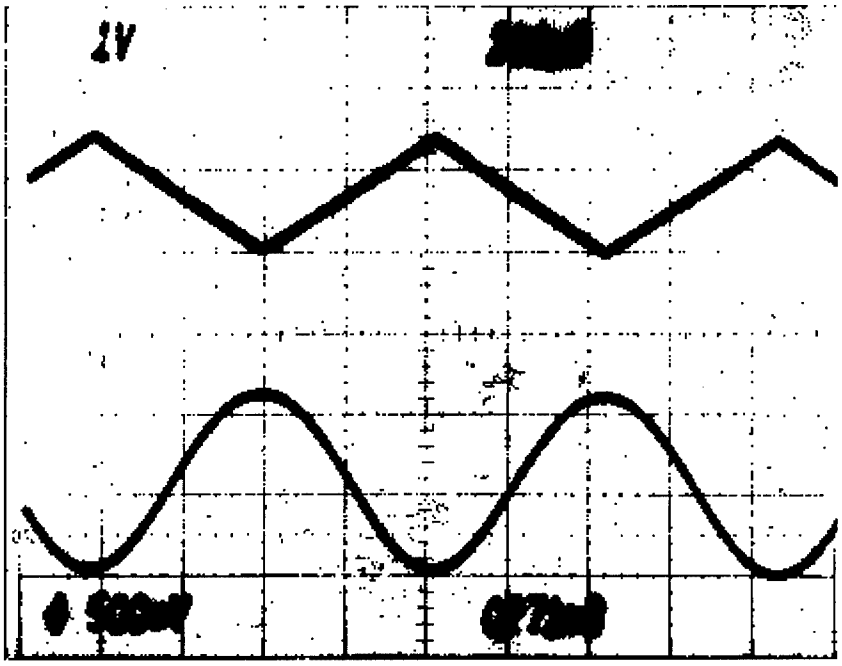

Figure 17: Transfer Function for a normal Mach-Zehnder, data.

For the carrier suppression modulator, the transfer function matched the first iteration device:

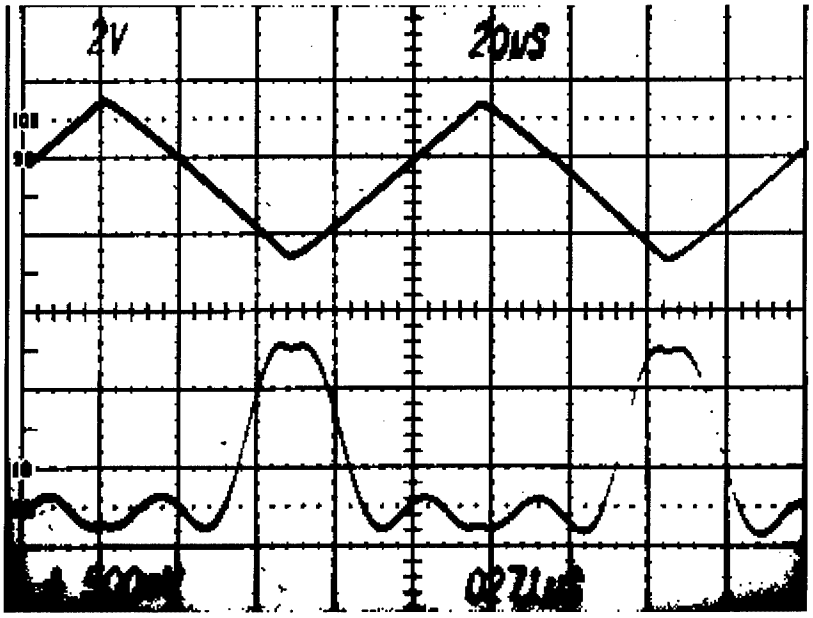

Figure 18, Second iteration suppressed carrier transfer function data.

The input triangle wave was intentionally overswept, so that the response curve could be shown before any inflection points of the input wavcform. Normally, the amplitude of the triangle wave has to be adjusted to match exactly one cycle of the transfer function. If one looks from the modulator major peak to second minimum, the same large max / small maximum characteristic is evident.

This modulator then had the pilot tone bias control attached. This is the same gated-tone bias control used at UTP for various product applications over the last 5 years. A two-tone was applied to find the operating OMI for this configuration. The two-tone spur was as shown, figure 19:

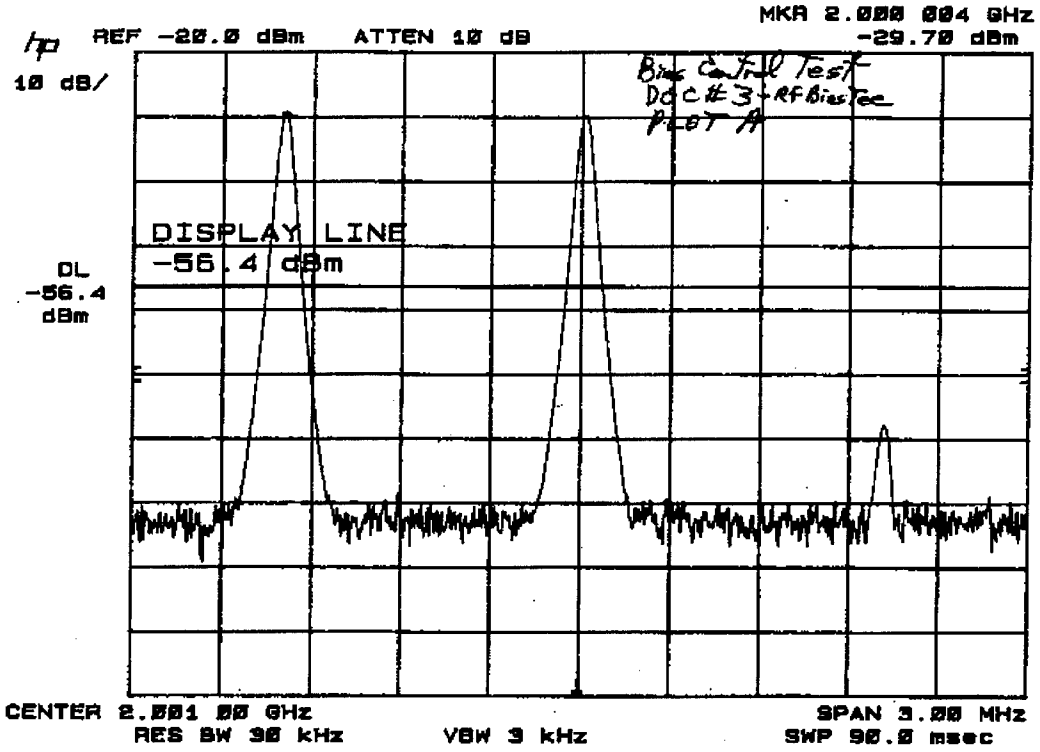

Figure 19, Bias control test data:

The spur was 47.7 dBc, corresponding to an OMI of 18.0% . The RF carrier was at -29.7 dBm. The second order was then measured at 4 GHz, shown in figure 20 before and after loop lock.

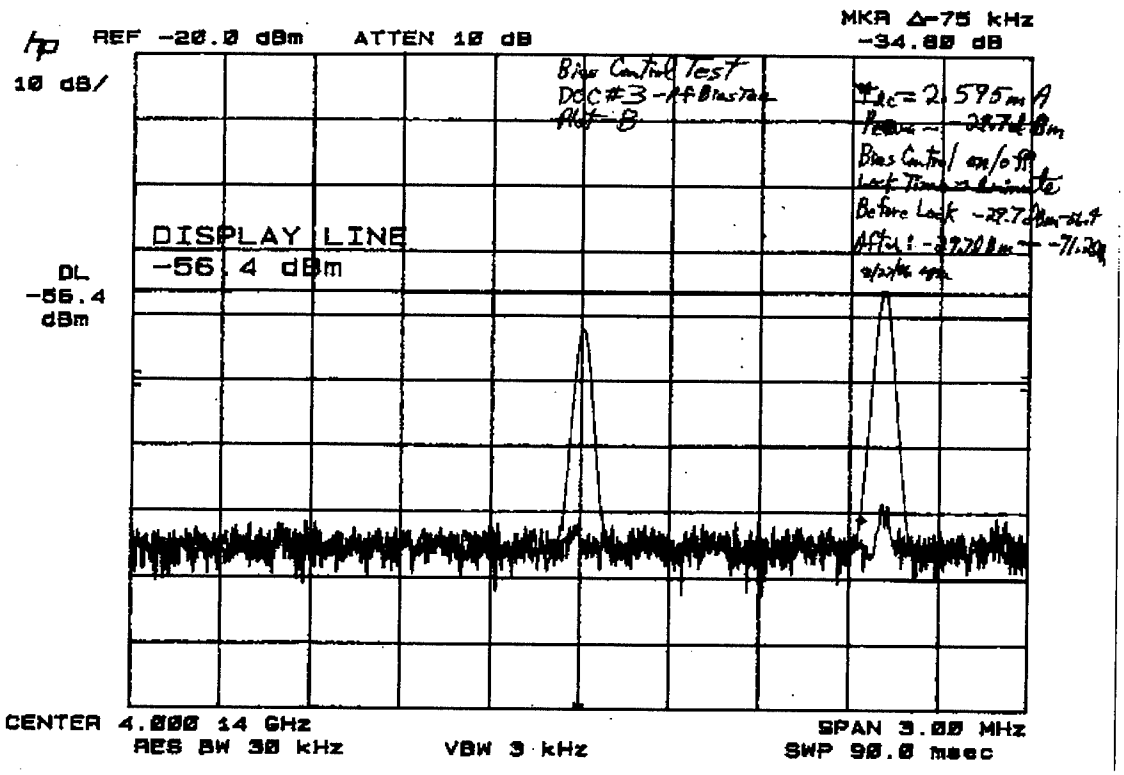

Figure 20, Second order distortion before and after loop null.

The settling time was approximately 1 minute, somewhat slow because of the large value of RF Vpi, but not unduly long. Before lock, the second order was 26.7 dBc, after lock, it hunted in and out of null, with peak distortions reaching -61.5 dBc. This corresponds to a bias point accuracy of 1.07 degrees of optical phase, for a normal MZ. Since this device is not a normal MZ, there might be some inaccuracy in stating the bias point stability in terms of sinusoidal phase offset, but this is representative.

This data shows a successful test of controlling the "inner" Mach-Zehnder of the carrier suppressed modulator, controlled by nulling distortions at the composite, or carrier suppressed output.

A photograph of the 19 inch rack breadboard is shown in figure 21:

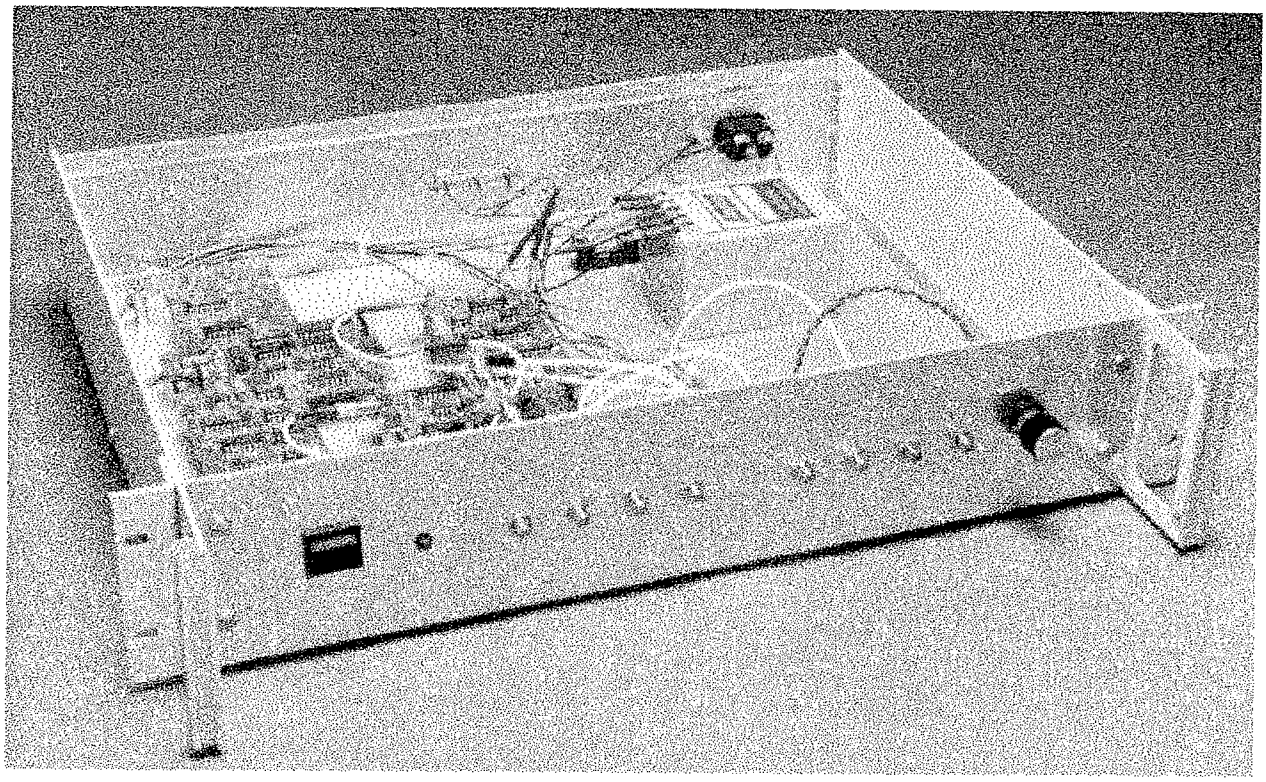

Figure 21: 19 inch rack breadboard electronics:

The two-tone test was then applied to both the simple MZ output, and the carrier suppression output, biased at full suppression. The normal MZ is shown here in figure 22:

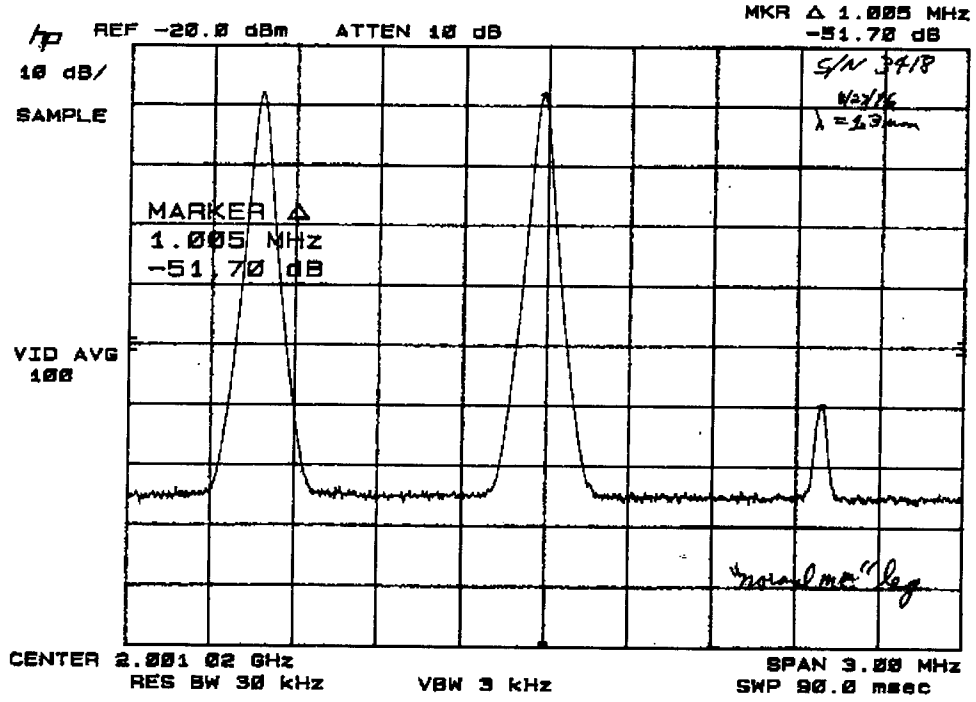

Figure 22, normal Mach-Zehnder two tone test:

OMI and Vpi can be calculated from the data. Idc=2.02mA, Pout = -28 dBm, spur = -51.7 dBc. RF applied was +7.2 dBm. OMI was calculated to be 14.37%. Using the ratio of the RF part to DC part to calculate OMI, 2.02mA and -28 dBm yields 12.5%. This is 1.2 dB lower than the spur method yields. Since this is the normal MZ leg, this information implies that there is 1.2 dB loss in the RF path, including the photodiode losses, and cable losses, along with any mismatch. Since the spur delta method is ratiometric, and not dependent upon specific absolute power levels, believing the spur calculation of OMI would imply that a 1.2 dB correction factor should be used to "calibrate" the AC/DC OMI calculation. We should consider in the evaluation of the more complex carrier suppressed configuration, the effects of this offset.

The carrier suppressed two tone is shown here, in figure 23:

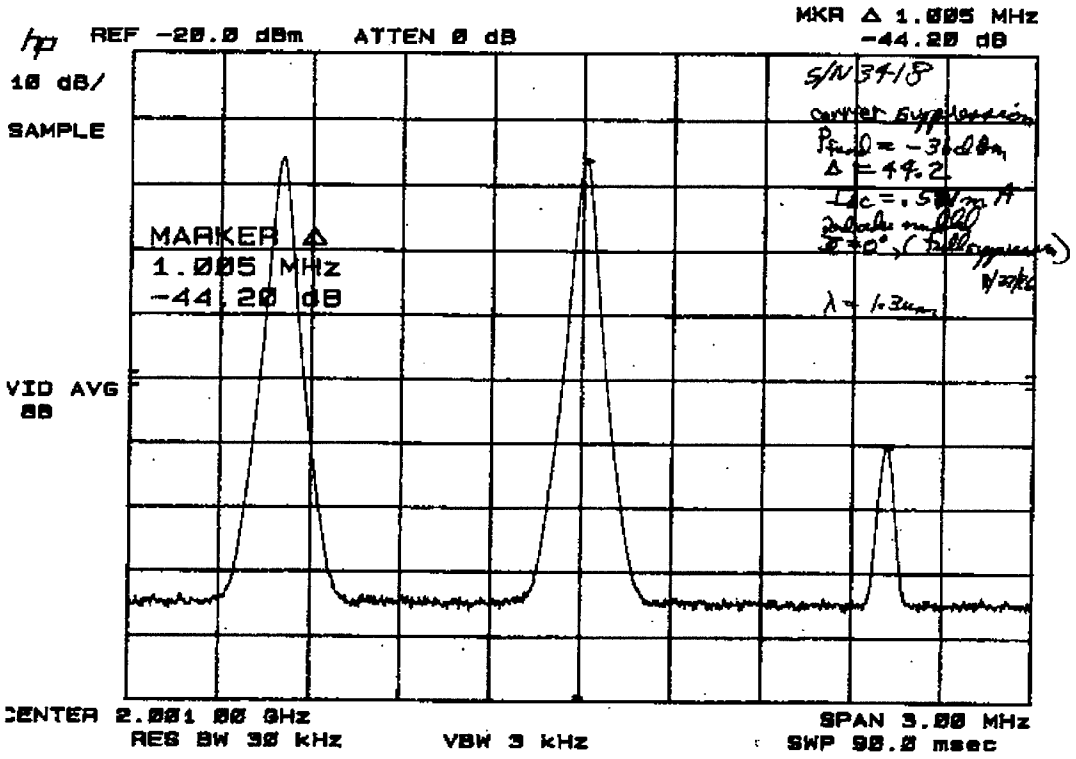

Figure 23: Carrier suppression two tone test data.

For the carrier suppressed test, the tone Pout was -36 dBm. The spur delta was -44.2 dBc, and the Idc was .521 ma. Pin was 7.2 dBm. Again, calculating OMI from both methods, the spur method yields an OMI of 22.13 %. Using the DC method, and correcting for the loss revealed in the normal MZ test, an OMI of 22.2 % was calculated.

SFDR measurements were conducted on the link, using a similar setup to that used for the iteration 1 testing. A two-tone test was conducted to evaluate IP3 for the optic link, and then a post-amp, an Avantek AFT-2064 was inserted after the photodiode to evaluate the link noise floor. The amplifier has a noise figure of 3.5 dB, an IP3 of +29 dBm, and a 42 dB gain. The fundamental gain of the two RF tones were measured to verify the amplifier noise characteristics. The noise floor with the optical power removed was measured to obtain the instrument noise floor.

The following, figure 24, shows the two-tone link linear output, and third order two-tone spur powers, both in dBm:

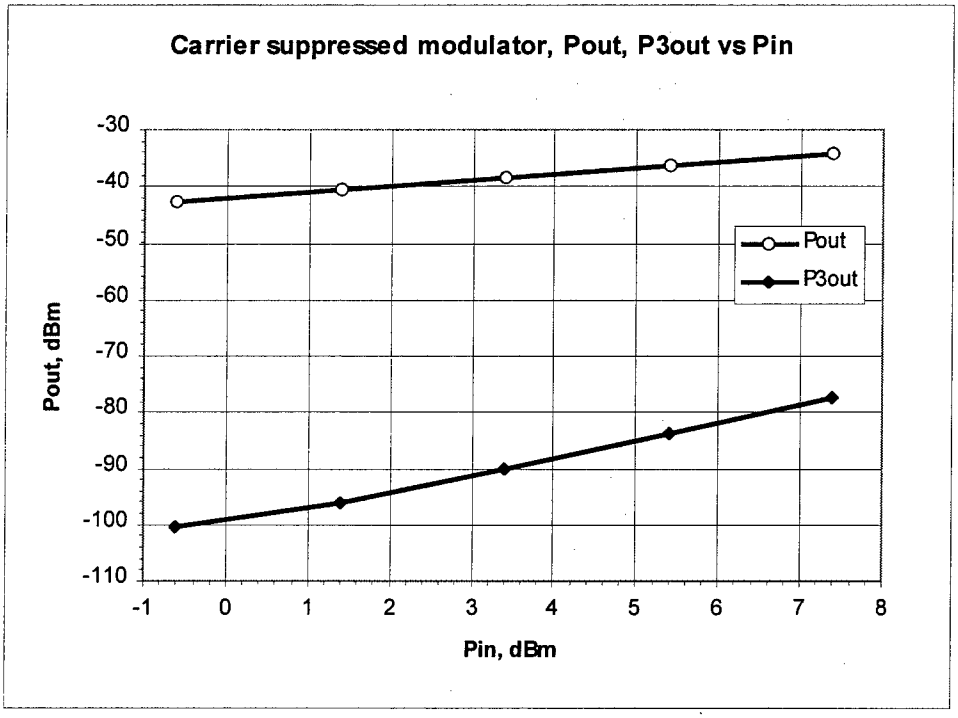

Figure 24, log-log plot of fundamental and third order distortion.

Of importance is that fundamental and third order terms follow 1dB/dB, and 3 dB/dB tracking with respect to the input power, which the data shows. This data was taken with .925 ma on the photodetector. The third order intercept at the output was calculated to be -12.9 dBm. Referenced to the input of the link, this yielded +28.9 dBm.

With the amplifier added, the link gain was then re-evaluated to +1.7 dB. This yielded an equivalent link IP3 of +30.6 dBm. The corresponding noise floor was measured to be -125.7 dBm(1Hz). When the optical power was removed, the noise floor dropped 5.4 dB. Using a noise power correction factor, the instrument noise floor delta gave a link noise power correction factor of 1.5 dB. This was used from tables in the HP 8566 spectrum analyzer manual, shown here, in figure 25.

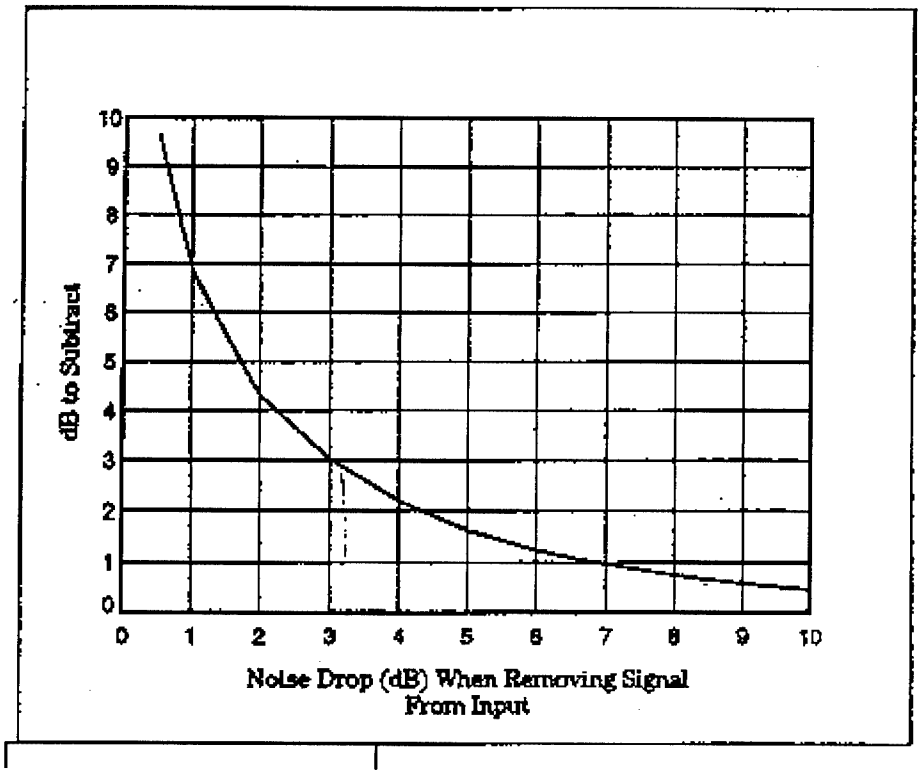

Figure 25, noise contribution from test equipment

The data arranged in composite for the link was then as follows:

Gain (with amplifier)	+1.7 dB
IP3 (neglecting amplifier IP3, but including amplifier gain:)	+30.6 dBm
Noise floor (with correction, amplifier noise removed)	-127.2 dBm(1Hz)
SFDR: 2/3 (30.6 - -127.2 dBm(1 Hz)) = 105.2 dB / (Hz)^2/3 Idc=.925mA	

UTP has published a performance parameter guide for use in designing externally modulated links. This is shown here in figure 26 for comparison to "normal" Mach-Zehnder modulators. This design chart dynamic range curves are shown only accounting for shot noise and thermal noise in the link. Any additional contributions such as laser RIN, or other link distortion or noise factors are not included. To compare this to a "normal" link, with other contributions, the following equations were used for a sinusoidal transfer function modulator:

Link Gain:

$$\text{Gain}(Io, Zload, Zmod) := 10 \cdot \log\left(\frac{\pi^2 \cdot Zmod \cdot Io^2 \cdot Zload}{Vpi^2}\right)$$

Third order intercept, referenced to input:

$$Pip3dBm(Vpi, Zmod) := 30 + 10 \cdot \log\left[\frac{(4 \cdot Vpi^2)}{Zmod \cdot \pi^2}\right]$$

Third order intercept, referenced to link output:

$$IP3out(Io, Zload) := 30 + 10 \cdot \log(4 \cdot Io^2 \cdot Zload)$$

Link noise figure:

$$Noisefigure(Io, Zload, Zmod) := \left[30 + 10 \cdot \log\left[\frac{(rin \cdot Io^2 + 2 \cdot q \cdot Io + inth(nf)^2) \cdot Vpi^2}{\pi^2 \cdot Io^2 \cdot Zmod}\right]\right] + 174$$

Link SFDR:

$$SFDR(Io, rin, inth, BW) := \frac{2}{3} \cdot 10 \cdot \log\left[\frac{4 \cdot Io^2}{BW \cdot (rin \cdot Io^2 + 2 \cdot q \cdot Io + inth^2)}\right]$$

An additional parameter used is the parameter inth, which is used here to represent the thermal noise contribution of the system, as well as the postamp noise figure contribution. This is used for convenience, since many integrated photodiode-preamplifier modules specify the noise at the input in units of pA/root-Hz. The following equation was used to calculate inth for the Avantek amplifier with 3.5 dB noise figure:

$$inth(nf) := \frac{10^{\left(\frac{nf}{20} - 10.2\right)}}{\sqrt{Zload}}$$

In a 50 ohm system, the equation reduces to a noise current equivalent to -174 thermal noise.

Other parameters in these equations are:

IP3out:	Third order two-tone intercept, expressed in dBm at the output of the link.
Zload:	The load impedance of the photodiode.
Io:	The DC photocurrent at the photodetector.
rin:	The laser rin, as a linear ratio. The 10 * log(rin) value used was -170 dBc/Hz
BW:	The measurement bandwidth, 1 Hz used here.
q:	Electron charge, 1.6 x 10^-19 coulombs
Zmod:	Modulator impedance
Vpi:	Modulator half wave voltage
SFDR:	Spurious free dynamic range, expressed in dB/Hz^(2/3)

Using the amplifier gains and noise figure, as well as the DC photocurrent of .925mA, the equations yield the following numbers, with the post amp gain added to IP3out, and link gain:

	"normal" MZ link (calculated)	Link performance, UTP "design chart"	"normal" MZ link + 42 db postamp.* (calculated)	Carrier suppressed modulator (data)	C.S.M. + postamp* (data)
Gain	-38.3 dB	-39,approx	3.7	-43.5	+1.7
Pip3input	30.7 dBm	-	30.7 dBm	+28.9dBm	+28.9dBm
IP3out	-7.7 dBm	-	34.3 dBm	-12.9 dBm	+30.6 dBm
Noise Figure	45.2 dB	45 ** dB	46.2 dB	45.1 dB	46.6 dB
SFDR dB/Hz^(2/3)	106.3	106.5	105.7	105.2	104.2

Figure 25a, simple MZ links and Carrier-suppressed link data

* Amplifier third order intercept not included in IP3, ** Design chart-subtract 3 dB for 50 ohm modulators

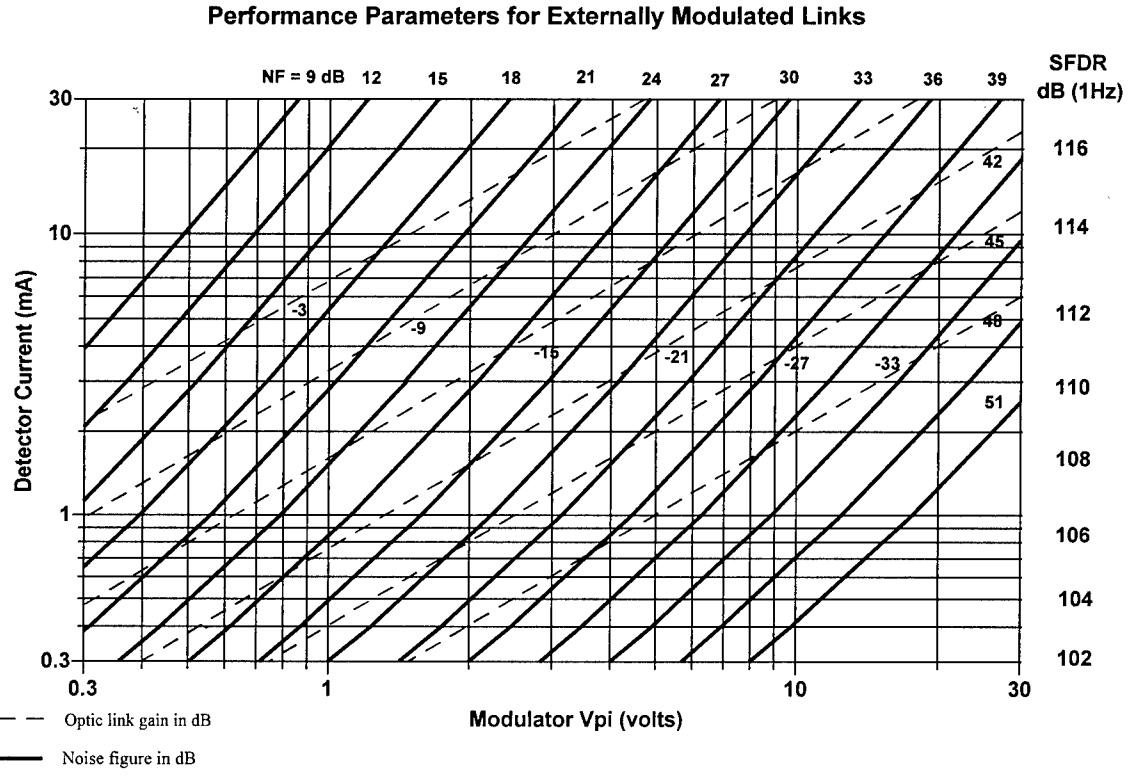

Figure 26, link performance of simple MZ

The carrier-suppression data shows very comparable performance, since the SFDR for a simple Mach-Zehnder in the .ma range should be no better than about 106 dB/(Hz)^2/3, from the shot noise and thermal noise limits alone. To be noted is the fact that the normal MZ is tabular data, and the Carrier suppressed configuration is actual data, with all of the incumbent "parasitic" contributions and measurement errors. It is thought that there might in fact be a slight advantage owing to the relative magnitude of gain and third order derivatives of the respective topologies. However, the differences seem to be very slight, and not easily revealed from the test data. Perhaps a more careful investigation of the analytical model in the beginning of this report, and more testing would provide more answers.

The RF swept frequency characteristics were evaluated on all devices. SN3419 is representative of the standard microwave modulators produced by UTP. The following plots were taken on S11, and S21 (e/o) for device SN3419, figure 27 and figure 28:

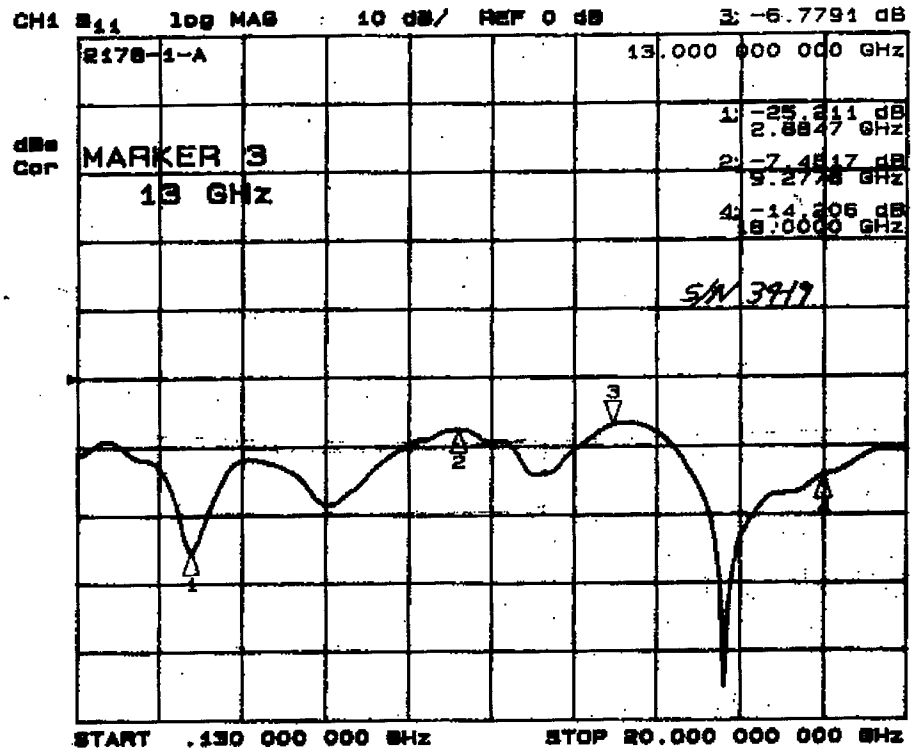

Figure 27: S11, SN3419

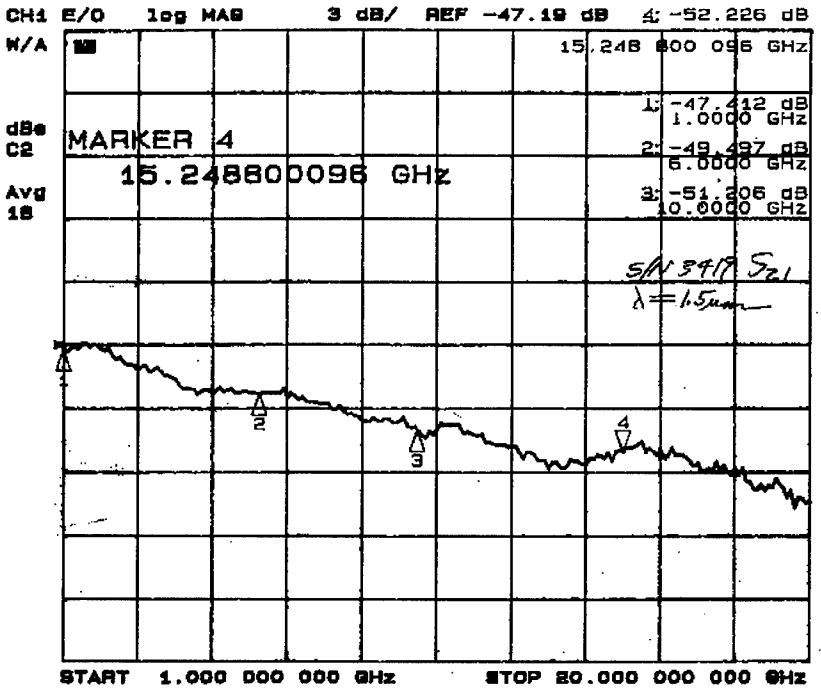

Figure 28: E/O response:

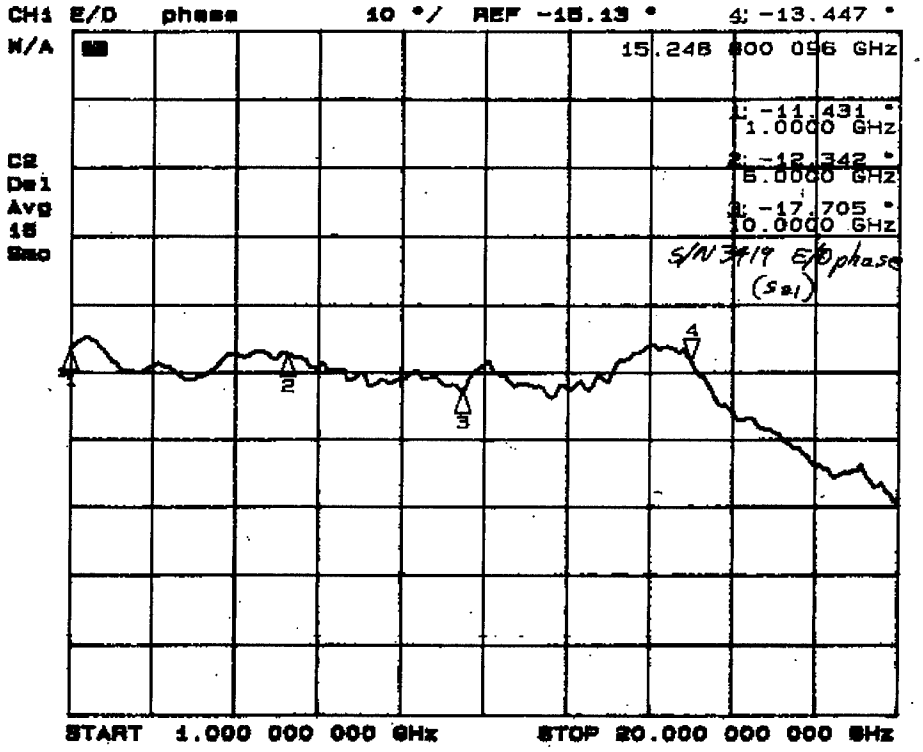

Figure 29: E/O phase:

S21 amplitude and phase, as well as S11 were normal for a configuration of this type. This structure was somewhat different than UTP 18 GHz modulators in that DC blocking capacitors were added to the RF terminations, which allowed use of a bias "tee" to supply the DC bias to the electrodes. Use of this DC blocking and bias "tees" are of particular importance in modulator topologies which require complex features, and hence, have limited room for additional DC electrodes.

A phase modulator was incorporated into SN3419 for linewidth modulation, which is of some interest in 1.5um wavelength applications. The phase modulator was swept for S11, which is plotted here:

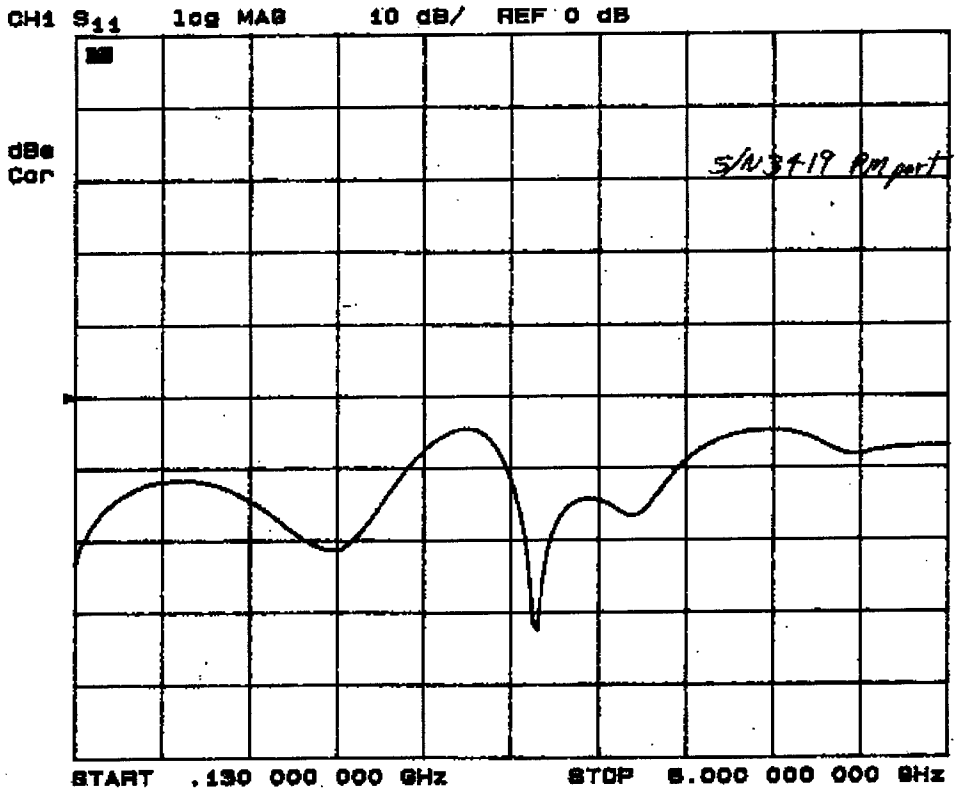

Figure 30, S11, Phase modulator input

The phase modulator exhibited usable bandwidth out to 6 GHz. For most linewidth modulation applications, return loss is not as important as the ability to couple high level power into the device, since linewidth modulation usually requires very high levels of phase modulation deviation factors.

INTEGRATED LOGISTIC SUPPORT (ILS).

The carrier suppressed modulators used for this program were developed from building block features found in UTP products. The packaging, internal interconnect technology, and design rules used to develop these modulators have been applied from other UTP products.

To this end, environmental performance, reliability, and ruggedness of these modulators should be identical to those standard products which are currently used in both military and commercial applications, by UTP customers.

All applications notes, and usage procedures defined for use of UTP standard product modulators should be directly applicable for these modulators.

SUMMARY

Several features with potential use in carrier suppressed modulator topologies resulted from this investigation:

- Bias schemes, control stability, and performance were investigated.
- Use of internally mounted photodiodes were investigated and shown to be feasible as a means of controlling the bias point of complex external modulator structures.
- Use of modulator circuit elements such as internal DC blocking components were investigated as a means of facilitating control of the bias point.
- The carrier suppression technique yielded comparable, or slightly improved SFDR over a simple modulator, which should might be explained with further study. However, use of these topologies to depart from normal sinusoidal transfer function characteristics may yield more design options for future applications.
- The suppressed-carrier modulator reveals itself as more of a modulator-within-a-modulator, since the output intensity from the "inner" MZ, (Mach-Zenhder), interferes again with the carrier suppression waveguide. This yields an interesting transfer function without the normal MZ relationships between fundamental, second order, and third order distortion characteristics.

ACKNOWLEDGMENTS

The authors wish to thank Norman Bernstein, of Rome Labs for his help in conducting this research. The authors wish to thank Robert Perusse, Karl Kissa, and Bill Merritt, of UTP, and Bill Bridges of Cal-Tech for their helpful comments and analysis.

REFERENCES

1. R. D. Estman, K. J. Williams, "Wideband Efficiency Improvement of Fiber Optic Systems by Carrier Subtraction," IEEE Photonics Technology Letters, Vol. 7, No. 2, pp. 218-220, February 1995.

2. Bridges, William. Caltech. unpublished analysis, 26 October, 1995

3. Montgomery, Robert "A Novel Technique for Double Sideband Suppressed Carrier Modulation of Optical Fields", IEEE Photonics Technology Letters, Vol.7, No. 4, April 1995.

4. Betts, G.E. "A Linearized modulator for sub-octave bandpass optical analog links," IEEE Trans. Microwave Theory Tech., vol. 42, pp. 2642-2649, 1994

APPENDICES

A: OMI and Vpi measurements

UTP

Uniphase Telecommunications Products
A Subsidiary of Uniphase Corporation

1289 Blue Hills Avenue
Bloomfield, CT 06002
Phone: (203) 769-3010
Fax : (203) 769-3007

Measurement of *OMI* Using the Third Order Two Tones of an Optical Modulator Having a Sinusoidal Transfer Function

Gregory J McBrien

Senior Staff, Technology Development

Christopher W. MacGregor

Technical Staff, Technology Development

BACKGROUND:

Measurement of optical modulation index (*OMI*) can sometimes be difficult if the DC and AC transfer function gains of the measurement system are not correlated. A method exists using the third order fundamental and intermodulation (intermods) tones of the sinusoidal transfer function of an interferometric optical modulator. Since the sinusoidal transfer function due to the interferometric nature of an external optical modulator is constant and predictable, the amplitude of a third order two tone spur with respect to the carrier is a direct function of the depth of modulation. This discussion reviews some of the background analysis present in the measurement relationships

ANALYSIS:

Given an external modulator having a sinusoidal response, the transfer function for 2 RF tones of equal amplitude is an odd function modeled by:

$$I_s = \frac{I_0}{2} + \frac{I_0}{2}\sin\left[\frac{V_m\pi}{V_\pi}\left[\sin(\omega_1 t) + \sin(\omega_2 t)\right] + \varphi\right]$$

where V_m is the zero to peak voltage of the RF tones, V_π is the voltage required to change the modulator output from off to on, and φ is a constant denoting the bias state of the device equivalent to $\frac{V_0\pi}{V_\pi} + \frac{\pi}{2}$ where V_0 is the bias voltage. For this measurement we must assume $\varphi = n\pi$ where n is an integer. If we expand the biased transfer function into a power series, keeping only the first and third orders, the simplified expression becomes:

$$I_s = \frac{I_0}{2} + \frac{I_0}{2}\left[\frac{V_m\pi}{V_\pi}\left[\sin(\omega_1 t) + \sin(\omega_2 t)\right] - \frac{1}{3!}\left[\frac{V_m\pi}{V_\pi}\left[\sin(\omega_1 t) + \sin(\omega_2 t)\right]\right]^3\right]$$

When we expand and simplify this expression and then use the trigonometric identities for $\sin^2(\theta)$ and $\sin^3(\theta)$ we can further simplify this equation in terms of just sin's of ω_1 and/or ω_2. This gives us the relative amplitudes of the two fundamental carriers, third order two tone spurs, third order harmonics, and third order intermods depicted in the graph below.

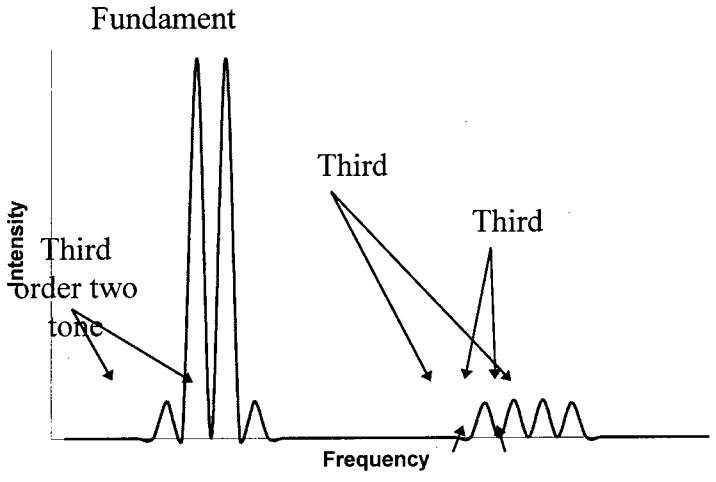

Figure 1: Two tones and third order harmonics.

By taking the ratio of third order two tone spur to the first order carrier, we can solve for OMI.

The ratio of the amplitudes is given by:

$$\frac{A_{2\omega_2-\omega_1}}{A_{\omega_2}} = \frac{\pi^2 V_m^{\,2} \sin(2\omega_2 t - \omega_1 t)}{\left(8V_\pi^{\,2} - 3\pi^2 V_m^{\,2}\right)\sin(\omega_1 t)}$$

However, when making measurements with analysis equipment, it is generally more useful to deal with *power* levels rather than amplitude levels. We will define this ratio of power levels between the carrier and third order spur depicted in the figure below as some variable Δ.

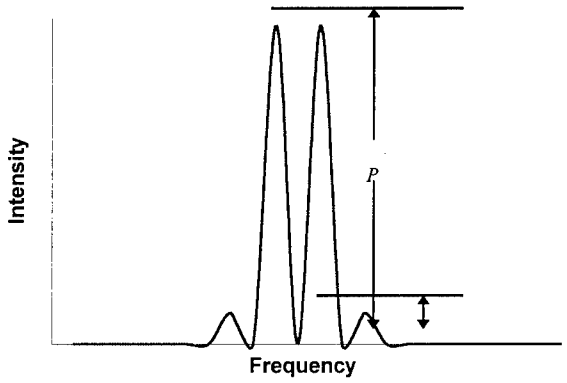

Figure 2: Ratio of carrier to spur defined as Δ.

Numerically, Δ can be defined as:

$$\Delta = \frac{P_{2\omega_2-\omega_1}}{P_{\omega_2}} = \frac{\pi^4 V_m^{\,4} \sin^2(2\omega_2 t - \omega_1 t)}{\left(8V_\pi^{\,2} - 3\pi^2 V_m^{\,2}\right)^2 \sin^2(\omega_2 t)}$$

If we look at the time average of amplitudes, the difference between carrier and spur amplitudes becomes:

$$\Delta_{avg} = \frac{\pi^4 V_m^{\,4}}{\left(8V_\pi^{\,2} - 3\pi^2 V_m^{\,2}\right)^2} = 20\ \log\left(\frac{\pi^2 V_m^{\,2}}{8V_\pi^{\,2} - 3\pi^2 V_m^{\,2}}\right)\ \text{dBc}$$

We can also use the equation for Δ_{avg} to solve for the third order intercept, or IP_3. By setting the argument of the log term in the previous equation equal to 1, and solving for V_m we can find the peak signal voltage theoretically required to reach IP_3.

$$V_m = \sqrt{2}\frac{V_\pi}{\pi}$$

To relate these equations to optical modulation index, or "OMI ", we will note that the first order component of the transfer function at the half power bias point is:

$$I_{s_{FO}} = \frac{I_0}{2} + \frac{I_0}{2}\left[\frac{V_m\pi}{V_\pi}\left[\sin(\omega_1 t) + \sin(\omega_2 t)\right]\right]$$

From this we can derive the peak amplitude value for each RF tone (ω_1, ω_2):

$$I_{s_{pk}} = \frac{I_0 V_m \pi}{2V_\pi}$$

It is prudent to note that we are not interested in the DC offset when looking at RF amplitudes. At the half power point, when $V_m = 0$, the optical output from this

expression is $I_0/2$, where I_0 is the maximum photo current at the peak of the interferometer intensity curve as seen in Figure 3:

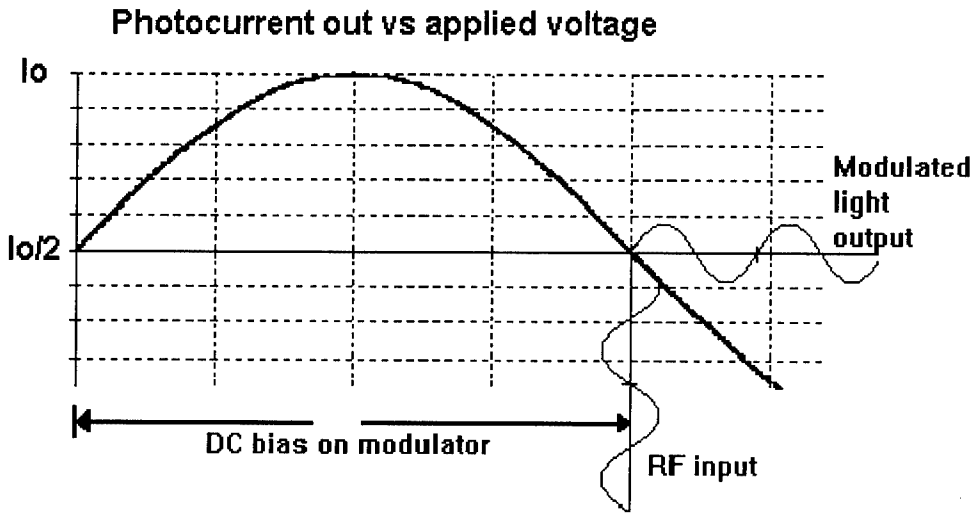

Figure 3: Modulator input to output transfer characteristic.

It can now be shown that the resulting ratio of RF peak amplitude to average DC value is given by:

$$OMI = \frac{\frac{I_0 V_m \pi}{2V_\pi}}{\frac{I_0}{2}} = \frac{V_m \pi}{V_\pi}$$

This equation will be used as the definition of OMI in this note. The last step in relating the measurement of the third order spur to the applied OMI is to solve the Δ_{avg} equation in terms of OMI using the definition stated above:

$$\Delta_{avg} = 20 \log\left(\frac{OMI^2}{8 - 3OMI^2}\right) \text{ dBc}$$

Hence, OMI can be found from the third order two tone spur height relative to the two tone carrier by:

$$OMI = \frac{2\sqrt{2} \cdot 10^{\frac{\Delta_{avg}}{20}}}{\sqrt{3 \cdot 10^{\frac{\Delta_{avg}}{20}} - 1}}$$

where Δ_{avg} is a negative number, spur relative to carrier, in dBc.

To summarize the analysis up to this point, a way to measure OMI accurately with an external modulator having a sinusoidal output is to simply apply two equal amplitude tones and measure the height of the third order two tone spur relative to the carrier. One requirement to remember is that the modulator must be biased at the half power point. This can be verified by minimizing the second harmonic content in the modulator output signal. In most high fidelity transmission applications the required accuracy for second order intercept is tight enough to ensure negligible errors from bias point setting. No DC measurement is required, nor is it necessary to relate the relationship between the DC and AC response of the photo diode, bias blocking "tee" or loss into the spectrum analyzer. Indeed, one use of a sinusoidal transfer function optical modulator can be to calibrate the receiving photo diode and receiving equipment for later precision OMI measurements.

Another method for measuring OMI involves directly measuring the zero to peak signal of a single RF tone and its DC level value. This will provide a direct measure of OMI. Referring to the definition of OMI stated earlier we see that:

$$OMI = \frac{I_{s_{pk}}}{I_0/2}$$

If one wants to directly measure the average DC and RF amplitude of the received signal, several errors can contribute to the measurement. The assumption of *OMI* measurement accuracy based on this technique is that the RF and DC response of the photo detector is known, and the RF loss through the photo diode output circuit and RF components is known. Additionally, any absolute loss error in the spectrum analyzer can lead to *OMI* errors. It should be noted that since the DC measurements of current from the photo diode are usually free from loss, the typical losses commonly found in the RF path will almost always yield a measured *OMI* value that is lower than the actual *OMI*. Problems such as a slow "tail" in the response of the perimeter regions of a photo diode can actually produce a much higher DC response than RF.

To make an accurate DC and RF measurement of the optical signal, the following steps should be considered.

1. Characterize or verify the DC and AC response of the photo diode. Manufacturers data can be useful.

2. Verify the DC load impedance on the photo diode. RF 50 Ω loads can certainly have significant deviation from 50 Ω.

3. Use an accurate network analyzer or other means to measure the loss of any components in the RF path such as bias "tees", connector adapters, and cables. Connector adapters to change an "N" series connector to an "SMA" connector can accumulate several tenths of a dB. Bias "tees" can have losses of 0.3 dB or greater.

4. Verify the absolute calibration of the spectrum analyzer. Applying an RF tone cross referenced to a precision RF power meter can provide a calibration data point.

Assuming the measurement errors are removed, the following relationship can be used to provide *OMI*:

$$OMI = \frac{\sqrt{\frac{2 \cdot 10^{\frac{P_{RF}-30}{10}}}{Z_{RF}}}}{\frac{V_{DC}}{R_{LOAD}}}$$

P_{RF} is the received RF power in dBm, Z_{RF} is the RF load, typically 50 or 75 Ω. V_{DC} is the DC voltage across the DC load resistor R_{LOAD}, often 50 Ω. This DC value must be for a modulator biased at the half power point. As an example, with 50 Ω loads and 0.25 volts on the detector average, -50 dBm measured by the spectrum analyzer will yield an OMI value of 4%.

In a particular test setup at UTP, RF loss through a bias "tee" and associated connectors was measured as 0.4 dB. If this were not corrected, the actual RF signal would actually have been (in this example) -49.6 dBm. The resulting OMI would then have incorrectly been 4.2%. Thus, small errors in measurement can produce noticeable errors in OMI.

B: Bias control interconnect and diagram

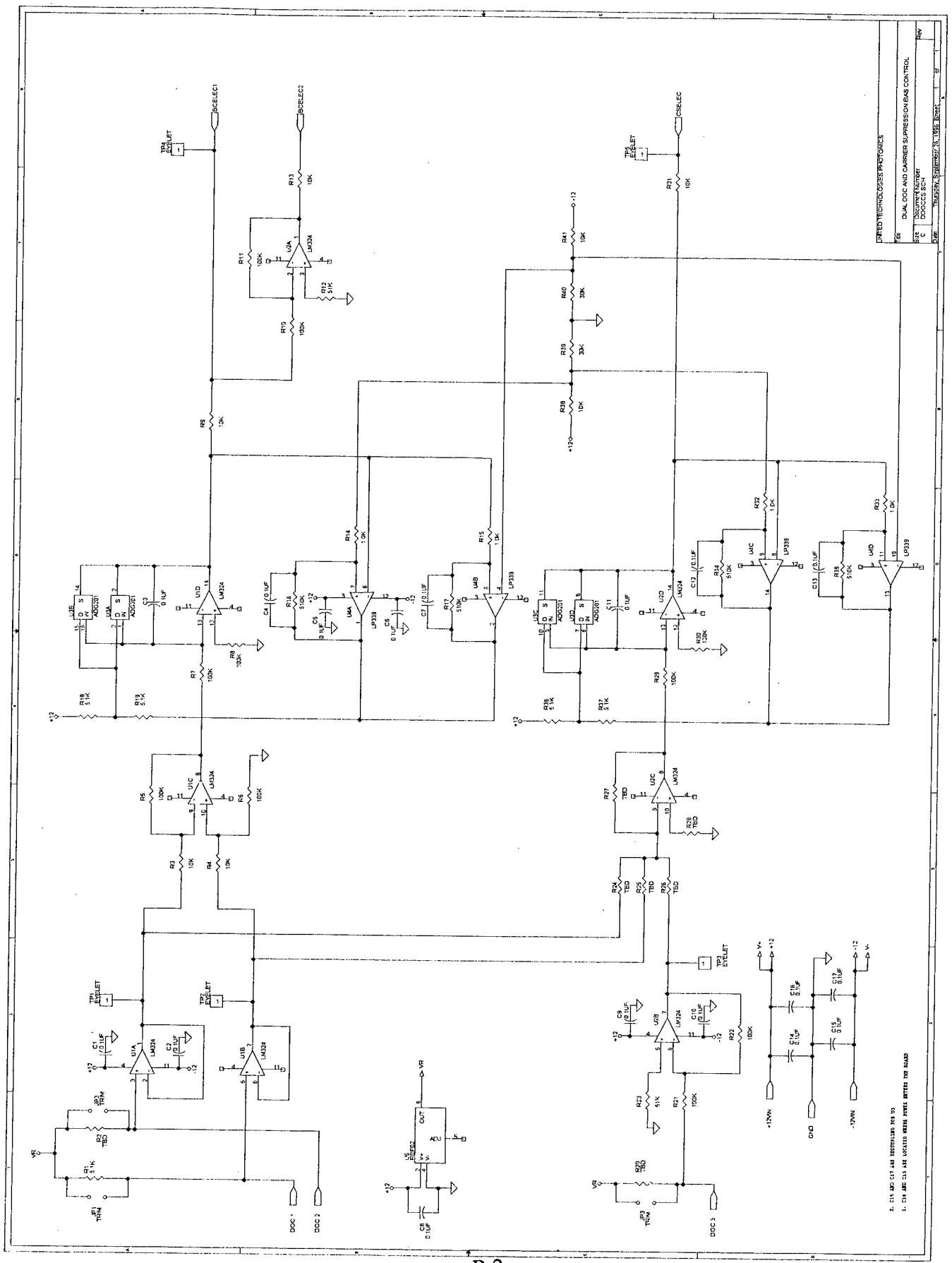

*U.S. GOVERNMENT PRINTING OFFICE: 1997-509-127-47204

MISSION OF ROME LABORATORY

Mission. The mission of Rome Laboratory is to advance the science and technologies of command, control, communications and intelligence and to transition them into systems to meet customer needs. To achieve this, Rome Lab:

a. Conducts vigorous research, development and test programs in all applicable technologies;

b. Transitions technology to current and future systems to improve operational capability, readiness, and supportability;

c. Provides a full range of technical support to Air Force Material Command product centers and other Air Force organizations;

d. Promotes transfer of technology to the private sector;

e. Maintains leading edge technological expertise in the areas of surveillance, communications, command and control, intelligence, reliability science, electro-magnetic technology, photonics, signal processing, and computational science.

The thrust areas of technical competence include: Surveillance, Communications, Command and Control, Intelligence, Signal Processing, Computer Science and Technology, Electromagnetic Technology, Photonics and Reliability Sciences.